Materials and Methods

Experimental methods

Plasmids and homologous recombination cassettes construction

All plasmids used in this study are listed in **Supplementary Table 1**. All plasmid constructions were performed by standard molecular biology techniques.

Creation of Renilla luciferase PCA cassette templates for homologous recombination: To construct *Renilla luciferase* Protein fragment Complementation Assay (henceforth Rluc PCA) templates, "Linker ((Gly. Gly. Gly. Gly.Ser)$_2$)-Rluc Fragments (F[1]:1-110aa; F[2]:111-310aa)" DNA sequences were PCR-amplified from yeast expression vectors that contain these sequences and subcloned into pAG25-linker-DHFR F[1,2] and pAG32-linker-DHFR F[3][31] plasmids between HindIII and XbaI restriction sites. This replaces linker-DHFR F[1, 2] fragment with linker-Rluc F[1] and linker-DHFR F[3] with linker-Rluc F[2] resulting in pAG25-linker-Rluc F[1] and pAG32-linker-Rluc F[2] followed by ADH gene terminator sequence (ADHter). Each of the above plasmids used to clone the linker-Rluc PCA fragments already contained unique antibiotic resistance cassettes that in the resulting constructs are 3' to the ADHter. Thus the final Rluc F[1] PCA template (pAG25-Rluc F[1]; Supplementary Table1) consists of pAG25-linker-Rluc

F[1]-ADHter followed by the TEF gene promoter and the Nourseothricin N-acetyl-transferase (*NAT1*) gene that confers resistance to Clonat and finally a TEF terminator.

The final Rluc F[2] PCA template (pAG32-Rluc F[2]; Supplementary Table1) consists of pAG32-linker-Rluc[2]-ADHter followed by TEF promoter, Hygromycin-B phosphotransferase gene (*HPH*) that confers resistance to Hygromycin-B and finally the TEF terminator. The above templates were used to PCR amplify homologous recombination cassettes to introduce Rluc PCA fragments 3' to the open reading frames-ORF, of the genes studied here.

Oligonucleotide design for PCR amplification of the Rluc PCA cassettes, their synthesis, PCR amplification and homologous recombination methods are identical to those described in our recent study[31].

As positive control for detection of protein-protein interaction (PPI) signal using Rluc PCA and as negative control for variation in signal upon α-factor pheromone treatment, neuronal nitric oxide synthase (nNOS) and aSyntrophin (aSyn) PDZ domains that are known to form a heterodimer[32] were used (results shown in Supplementary Figure 7). These PDZ domains are foreign to yeast. PDZ-linker-Rluc PCA fragment fusions were expressed from a plasmid under the control of the TEF promoter and by maintaining the same resistance for each fragment as on endogenously tagged proteins (i.e. Clonat for Rluc F[1] and Hygromycin for Rluc F[2]). To make these constructs, nNOS and aSyn PDZ domain DNA sequences were PCR-amplified from pCB015 and pSH71 plasmids (a kind gift from W.A. Lim, UC San Francisco) and cloned into p41NAT-linker-Rluc F[1] and p41HPH-linker-Rluc F[2] plasmids, respectively between XbaI and BspEI sites present 5' to the linker. These result in plasmids p41NAT-nNOS-

linker-Rluc F[1] (pMM50; Supplementary Table1) and pHPH-aSyn-linker-Rluc F[2] (pMM51), respectively.

Ste5 Rluc PCA constructions: To measure the dynamic equilibrium of Fus3-linker-Rluc F[1]:Ste5-linker-Rluc F[2] (henceforth Fus3-Ste5) interaction by Rluc PCA and to measure active levels of Fus3 (Fus3pp) by western blotting in various mutant forms of Ste5, *STE5* was expressed from a plasmid under the control of its own endogenous promoter in a Ste5 knockout *MAT***a** strain (*ste5*Δ) and Fus3 gene being endogenously fused with linker-Rluc F[1] (pRS316 plasmids expressing $Ste5^{WT}$ (pSH95) and $Ste5^{ND}$ (pRB200) are gifts from Dr. W. A. Lim[9]); (MM003 strain; Supplementary Table 2).

To construct Rluc PCA fusions in the above plasmids, linker-Rluc F[2] PCA fragment was fused to 3' of Ste5 variants ($Ste5^{WT}$ and $Ste5^{ND}$). For this purpose linker-Rluc F[2] along with ADHter was PCR amplified from pAG32-Rluc F[2] (Supplementary Table1). The 55 bp sequence at the 3' of *STE5* ORF (excluding the stop codon) was introduced as part of the forward oligonucleotide in order to make use of the XhoI restriction site available at 3' of *STE5* ORF. The PCR product containing 55bp of *STE5*, linker-Rluc F[2]-ADHter sequence was subcloned between XhoI and BamHI restriction sites on pSH95 and pRB200 plasmids to obtain pSH95-MM100 and pRB200-MM113, respectively (Supplementary Table 1).

Venus PCA plasmid construction: To detect and visualize the precise localization of Ste5 interaction with Ptc1, we utilized the variant of PCA based on a variant of Yellow fluorescent protein (Venus). For this purpose both Ste5 and Ptc1 fused to Venus PCA

fragment 1 and 2 (VF[1] and VF[2]) respectively were constitutively over expressed under the ADH promoter from plasmids. To make these constructs, *STE5* and *PTC1* ORF sequences were PCR-amplified from Yeast genomic DNA and subcloned into multiple cloning sites (MCS) of p413-L-VF[1] and p415-L-VF[2] plasmids between XbaI and BamHI restriction sites (Supplementary Table 1).

Plasmids for localization of Ste5 mutant forms: To test whether the phosphosite mutations on Ste5 full length protein affects its normal localization during the mating response we fused full length Venus (variant of Yellow florescent protein) at c-terminal of Ste5. The plasmids (used for Supplementary Figure 14; listed in supplementary table 1) were created in the same way as described above for pSH95-MM100 and pRB200-MM113 but Rluc F[2] is replaced with full length Venus.

Construct for over-expression of Ptc1: To test the morphological pathway output and measure levels of Fus3pp under increased phosphatase (Ptc1) concentration in *MAT***a** cells (for Fig 4 & Supplementary Figures 15, 27), Ptc1 was constitutively over-expressed under control of the ADH promoter on pMM60 plasmid. To make this construct, *PTC1* ORF sequence was PCR-amplified from Yeast genomic DNA and subcloned into a multiple cloning site (MCS) of p415 between XbaI and BamHI restriction sites.

Constructs for in vitro protein purifications: To detect Fus3p mediated phosphorylation of individual phosphosites on Ste5_pep2 variants (for Supplementary Figure 9; see main text for description of Ste5_pep2 phosphosite mutants), *In vitro* kinase assays were

performed using GST-Fus3p and GST-Ste5_pep2 (residues 214 to 334) fusion proteins purified from *E. coli* cells. N-terminal GST fusion of Fus3 was made by PCR-amplifying *FUS3* ORF sequence from Yeast genomic DNA and cloning it between BamHI and EcoRI restriction sites of MCS on pGEX-5X-3 vector (Amersham). To create N-terminal GST fusions of mutant Ste5_pep2 peptides, DNA sequence for amino acids 214 to 334 were PCR-amplified from a different plasmid template for each mutant (Supplementary Table1: $ABCD^{WT}$; pSH95-MM100, Abcd; pSH95-MM108, aBcd; pSH95-MM109, abCd; pSH95-MM110, abcD; pSH95-MM111 and abcd; pSH95-MM112). Each PCR product was separately cloned into pGEX-5X-3 plasmids between BamHI and XhoI restriction sites. Similarly, to generate plasmids with N-terminal MBP fusions of Ptc1 and Fus3, their ORF sequences were PCR-amplified from the Yeast genomic DNA and cloned in to pMAL-c2x plasmid vector (New England Biolabs) between BamHI & HindIII and EcoRI & XbaI restriction sites respectively (pMM216 & pMM217).

All plasmid constructs were verified by standard sequencing methods.

Yeast strains: All Yeast strains used in this study are shown in **Supplementary Table 2**.

Mutagenesis

The significance of each Ste5 phosphosite on Fus3-Ste5 interaction dynamics, Fus3 phosphorylation and morphological pathway output were characterized using various phosphosite mutants of Ste5. In one series, combinations of non-phosphorylatable mutants were generated for all four sites and in another two sets, combinations of pseudo-phosphorylated mutants were generated.

To make non-phosphorylatable mutants of Ste5, Threonines (T) were mutated to Valine (V) and Serines (S) to Alanine (A), while pseudo-phosphorylated mutants were generated by mutating both Threonines and Serines to Glutamic acid (E). Mutagenesis was carried out by using standard Site-Directed mutagenesis (Quick Change Site-Directed Mutagenesis Kit- Stratagene # 200519) following the manufacturers instructions. For both series of mutations, first single site mutations were generated using pSH95-MM100 as site-directed mutagenesis PCR template. To generate double site mutations the single site mutated plasmids were used as templates. Similarly to make triple mutations the double site mutated plasmid templates and to generate *STE5* with all four sites mutated, triple site mutated plasmids were used as PCR templates. The presence of correct mutations for all combinations was verified by sequencing.

Similarly, to disrupt the recruitment of Ptc1 to Ste5, Ste5 amino acids from 277 to 280 were mutated to Alanine.

Generating 3' Rluc PCA fragment fusions with endogenous genes

To study the protein-protein interaction dynamics by Rluc PCA with proteins expressed at their native levels and without over-expressing them (For Figs. 2 & 4), PCA fragments were fused to 3' of gene of interest preceded by linker sequence at their chromosomes by using standard homologous recombination methods[33]. Design of oligos, PCR amplification of the cassette, transformation of yeast competent cells with PCR product for homologous recombination and verification of the correctly tagged genes by colony PCR were performed as described in our recent study[31], with the exception that

instead of DHFR fragments, we amplified and created fusions with Rluc PCA fragments using Rluc PCA templates (pAG25-Rluc F[1] and pAG32-Rluc F[2]).

Since pheromone response is absent in diploid yeast cells, fusion of both Rluc F[1] & F[2] to two genes of interest was carried out in the same haploid strain (*MAT***a**; BY4741). In order to do this, we first created fusion of Rluc F[1] cassette to the first gene of interest (for example *FUS3*). Positive transformed cells were selected for Clonat antibiotic resistance and further verified by colony PCR. Verified clones were made chemically competent followed by transformation with the Rluc F[2] cassette PCR product specific for the second gene of interest (for example *STE5*). After a second transformation, clones were first selected using double antibiotic selection for both fragments (i.e., plates with Clonat and Hygromycin antibiotics) followed by further verification of correct 3' fusion of PCA fragments with specific genes by colony PCR.

In order to verify that the fusion of PCA fragments to C-terminal of Fus3 and Ste5 proteins do not interfere with their normal expression levels strains expressing fusion proteins were tested for their normal expression using Rluc fragment specific antibodies (Supplementary Figure 13). To test if expression of fusion proteins disrupts their normal physiological function in response to pheromone stimulation, morphological response was measured under non-stimulated and stimulated conditions (data not shown). No significant change in expression or pathway responses were detected with genes expressed as fusions to PCA fragments whether they were expressed from chromosomes or from the plasmids (in the cases of $Ste5^{WT}$ and Ste5 mutants).

Rluc PCA luminescence detection

All protein-protein interaction signals using Rluc PCA were measured using cells equivalent to 0.1 OD_{600} (approximately $1x10^6$ cells). This was the minimal and optimal cell density required by Rluc PCA signal detection and to measure protein interaction dynamics among MAP Kinase signaling proteins (data not shown). Cells were grown in either Low Fluorescent Media (LFM) complete[34] or appropriate selective medium overnight to make a pre-culture. From the pre-culture, fresh cultures were started at an OD_{600} of 0.05 or less and allowed to grow up to 0.1 OD_{600} at 30ºC with shaking. For each sample, cells equivalent to 0.1 OD_{600} were spun, supernatant was discarded and cells were resuspended in 160 µl of fresh medium. Cells were transferred to white 96-well flat bottom plates (Greiner bio-one # 655075). The Luciferase substrate Benzyl-Coelenterazine (Nanolight #301) was diluted from the stock (2 mM in absolute ethanol) using 1x phosphate-buffered saline (PBS), pH 7.2 containing 1 mM EDTA (10x PBS stock (1.4 M NaCl, 27 mM KCl, 100 mM Na_2HPO_4, 18 mM KH_2PO_4, pH 7.3) is diluted to 1x using deionized water). Pheromone α-factor (Zymo Research #Y1001) dilutions were prepared in 0.1 M sodium acetate. An LMax II^{384} Luminometer (Molecular Devices, Sunnyvale, CA, USA) was used to measure the protein-protein interaction signal.

Using the internal injectors of the Luminometer, 20 µl each of substrate (to a final concentration of 10 µM) and appropriate dilutions of α-factor or medium alone without α-factor, but with equivalent sodium acetate (to non-treated samples) were added to the cell mixture, mixed by shaking and incubated for 60 seconds. After incubation, Rluc PCA signal was integrated for 30 seconds. In a single experiment, for each sample, signal was

measured in triplicates and in total, experiments were repeated independently three times. Standard error of the mean (SEM) were calculated from the mean values of three independent experiments and shown as error bars for all relevant results.

In order to determine Rluc PCA signal from background luminescence for all α-factor dose-response, single concentration stimulus and kinetics data, first, the luminescence signal of medium, substrate alone and the background luminescence of *MAT***a** cells were subtracted from every measured signal to obtain the net luminescence. Second, α-factor was dissolved in 0.1 M sodium acetate and dilution of acetate resulted in a small linear decrease in substrate stability, resulting in an apparent 8.157% decrease in signal. In order to account for this, we applied a correction of 8.157 % to net PCA luminescence signal.

Western analysis to detect Fus3 phosphorylation

Cells were grown overnight to saturation in YPD or appropriate selective medium. Overnight cultures were used to start fresh 250 ml culture starting at cell density of 0.05 OD_{600} or less and grown to 0.1 OD_{600}. Cells were stimulated with α-factor for 15 minutes, spun for 5 minutes at 500xg, supernatant was discarded, the pellet washed with sterile water, spun again and frozen at -80ºC. Frozen pellets were thawed on ice, resuspended in 500 µl of Yeast protein extract buffer containing protease inhibitors. Buffer composition was adopted from Andersson et.al.[35] with some modifications; 10% Glycerol v/v, 15 mM EDTA, 15 mM $MgCl_2$, 1 mM DTT, 0.1% Triton X-100 v/v, 250 mM NaCl, 1 mM NaN_3 in 25 mM Tris-Cl pH=7.4. In addition, phosphatase inhibitor: 0.25 mM Sodium ortho-vanadate and protease inhibitors (PMSF-1 mM, Pepstatin A 5

µg/ml, Leupeptin 5 µg/ml and protease inhibitor cocktail (Roche Diagnostics # 11873580001)

To the above cell suspension 250 µl of glass beads were added and the mix was vortexed for 1 minute, 5-6 times with 1 minute intervals of incubation on ice. Vortexed cell mix was spun at 10,000xg for 10 min at 4ºC, cell lysate (supernatant) was aspirated into a new vial. An aliquot of lysate was used for SDS-PAGE and the rest was stored at -80ºC. Standard methods were used for the SDS-PAGE and western blotting experiments. Samples were run on 12% SDS-PAGE gel. Proteins from the gel were transferred to PVDF membranes using semi-dry transfer method. After the transfer, the membrane was blocked with 5% milk solution in Tris buffered saline and 0.2% Triton X-100 (TBST) for one hour at room temperature (RT). Following this, blots were probed with primary anti-phospho MAPK antibody (Cell signaling; Phospho-p44/42 MAP Kinase antibody #9101) in 5% w/v bovine serum albumin (BSA) solution at 4ºC overnight with gentle shaking. Blots were then washed three times with TBST, each wash for 10 minutes at RT on a rocker. Following the wash, blots were incubated with a secondary antibody (Cell signaling #7074) in 5% milk solution in TBST for one hour at RT. Then the blots were washed three times with TBST. Electrochemiluminescent reagent (PerkinElmer, # NEL 104 and NEL 105) was added to the blots and allowed for 60 seconds on bench. Excess ECL reagent was removed and blots were then exposed to film (GE Healthcare #28906838) and the films were developed on a KODAK M35A X-OMAT processor.

Stripping the blots and probing for loading control: In order to strip the antibodies from blots, they were incubated in stripping buffer (62.5 mM Tris-Cl pH=6.8, 2% SDS w/v

and 100 mM β-Mercaptoethanol) at 60-65ºC for 45 minutes with occasional shaking. Then blots were washed 4-5 times with TBST. Stripped blots were blocked with 5% milk in TBST for 1 hour at room temperature followed by probing the common and abundant protein in yeast, 3-Phosphoglecerate Kinase (PGK) using anti-PGK antibody (Molecular Probes # A6457).

Analysis of different morphological phenotypes

Cells were grown overnight in Low Fluorescence Medium (LFM) either complete or containing selective antibiotics to make a pre-culture. From the pre-culture fresh 3 ml cultures were started beginning at 0.05 OD_{600} or less cell density and grown at 30ºC with shaking up to 0.1 OD_{600}. Cultures were treated with indicated concentrations of α-factor pheromone and continued to incubate at 30ºC with shaking. To avoid heterogeneities from different stages of the cell cycle, α-factor treated cells were incubated for 3 to 4 hours before taking the images.

Preparation of microscopy plates; For image acquisition by microscopy, 96-well optical quality clear bottom plates (NUNC #164588) were used. In order to attach the cells to the bottom of wells, lectin Concanavalin A (ConA; Sigma # C-2631) was used as a cell binding agent. Each well was coated with 0.1 % ConA w/v at room temperature for 15 min. Then, the ConA solution was aspirated and wells were washed once with deionized sterile water. In order to activate the ConA, a solution of 20 mM $CaCl_2$ and 20 mM $MnSO_4$ was added to each well and incubated for another 15 minutes at room temperature followed by a wash with deionized sterile water. Cell suspension was added

to wells and allowed to attach for 10 min. Differential Interference Contrast-DIC, images were acquired on a NIKON eclipse TE2000-U inverted microscope connected to a CoolSNAP-fx CCD camera (Photometrics, Pleasanton, CA, USA) using a 60X DIC H Plan APO Oil objective. Image acquisition was done with Metamorph software (Molecular Devices, Downingtown, PA, USA).

Image Analysis and classification of phenotypes: Before we did any morphological response analysis, we observed under the microscope for 'over-time development or change in morphologies' after treating the cells with different concentrations of alpha-factor. We took images every 15 minutes starting 30 minutes after stimulation until 6 to 8 hours. In addition to determining the optimal time for imaging, over-time development of morphologies also helped us to clearly classify the morphologies into different categories (i.e. axial budding, bipolar budding, cell-cycle arrested and shmooing). Movie files generated from the time series images are included in Supplementary Figure 2 (requires the latest version of Adobe reader (9 and above) to view the movies).

As seen in the movies, after 4 hours of stimulation with 0.1 μM alpha-factor, cells rapidly recover from the Bipolar budding state and start to re-bud normally (i.e. axially). When stimulated with 1.0 μM α-factor, shmooing state is maintained until 5 hours, after which cells slowly start to re-bud. For all the morphology analysis in the paper, images were taken between 3 to 4 hours of time after stimulation, which was also the optimal time to distinguish morphologies. No re-budding phenotype was observed within this time period.

We have performed all the experiments in *BAR1* intact cells (BY4741 strain). Since we focused on the final cell fates of pheromone response, it was very important that we do not make the strains more sensitive (by deleting *BAR1* gene) to α-factor than normal wild type cells. In order to avoid the heterogeneity that might be caused by Bar1 mediated degradation of α-factor in the medium and to keep the results consistent, we undertook the following precautions:

1. As seen with the over-time development of morphologies, cells start to recover from the pheromone response after 4 to 5 hours of stimulation (Supplementary Figure 2). Since Bar1 is mainly shown to help cells recover from pheromone arrest which could affect the rate of recovery of different morphologies, we avoided taking images after 4 hours of stimulation.
2. We optimized and reduced the cell-density to the minimum that would result in large dilution of the available Bar1 in the medium. For both morphology and Rluc PCA assays, fresh cultures were made the next day from the overnight cultures and allowed to grow till very minimal cell-density (OD_{600} 0.05 to 0.1) that was optimal for both the assays. In case of Rluc assays, cells were again resuspended in fresh medium thus further removing the Bar1, if any present in the medium.
3. Whenever possible aliquots from the same fresh stock of α-factor was used for related experiments in order to avoid any was irregularities from batch to batch of α-factor.

During image analysis cells were manually classified in to 4 different phenotypes; axial budding, bipolar budding, cell cycle arrested and shmooing. The phenotypes were distinguished in the following manner: axial budding; normal round cells (3-5 μM

diameter) with daughter cells (buds) appearing axial to previous budding site. Bipolar budding; round cells with daughter cells appearing in the opposite direction to the previous budding site resulting in a chain of cells attached together. Cell cycle arrested; enlarged cells with larger average size (5-8 μM) compared to budding cells and Shmooing; pear shaped cells that are elongated and with active extension called shmoo. Anywhere from 500 to 1,500 individual cells were counted from 10 to 15 images taken per sample and sorted into either of the above four categories. Fractions of different phenotypes (percentage) were calculated from the total number of cells.

Protein purifications

GST-fusions of Fus3, mutant variants of Ste5_pep2 (WT, Abcd, aBcd, abCd, abcD and abcd) and MBP fusions of Fus3 and Ptc1 were purified from Rosetta (DE3) strain of *E.coli*. Cells transformed with appropriate plasmid were grown overnight to make a pre-culture from which fresh 500 ml cultures were started. Cells were grown up to 0.6 OD_{600} at 37ºC with shaking. To induce over-expression of fusion proteins, cells were treated with 1 mM Isopropyl-β-D-thiogalactoside (IPTG) and allowed to grow at 18ºC with shaking for 12 to 14 hours. Then, cells were harvested by centrifugation, resuspended in PBS containing protease inhibitors, lysed by sonication, spun and cell-lysate was aspirated. From cell-lysates, GST-fusion proteins were purified using Glutathione Sepharose 4B (GE Healthcare #17-0756-01) column and MBP-fusion proteins using the Amylose Resin (New England Biolabs #E8021S) following the manufacturers instructions. Purified proteins were buffer exchanged with 20 mM Tris-Cl.

pH=8.0, 150 mM NaCl and 2 mM $MgCl_2$ overnight at 4ºC. Buffer exchanged proteins were either directly used for the kinase assay or aliquoted and frozen at -80ºC.

In vitro Kinase assay

In order to detect partially active Fus3 (Fus3p) mediated phosphorylation on all four individual phosphosites present on Ste5, various mutant forms of Ste5_pep2 were used; for each site a peptide was generated wherein all but one phosphosites were mutated to non-phosphorylatable form (Supplementary Table 1). In wild type peptide, no sites were mutated while in "abcd" peptide all four sites were mutated to the non-phosphorylatable form (Ser or Thr->Ala). These peptides were used as positive and negative controls respectively in the *in vitro* kinase assay.

Fus3 purified from *E.coli* has been shown to be phosphorylated on Tyrosine (Y182) of its activation loop[36]. The tyrosine phosphorylated form of Fus3 has also previously been shown to possess partial kinase activity[9]. Hence, to detect Fus3p mediated phosphorylation of individual phosphosites of Ste5, purified GST-Fus3p was used without any modifications. In *in vitro* kinase assays, purified GST-fusions of individual mutants (all from 214-334 amino acids) of Ste5_pep2 (1.0 μM) were incubated with GST-Fus3p (0.5 μM) in 100 μl of kinase reaction buffer (20 mM Tris-Cl, pH=8.0, 150 mM NaCl, 2 mM $MgCl_2$, 0.1% IGEPAL (tert-Octylphenoxy poly(oxyethylene)ethanol), 2mM TCEP (Tris[2-carboxyethyl] phosphine)) containing 0.5 mM ATP and 10 μCi of γ^{32}P-ATP (PerkinElmer # BLU002Z). As controls, one mix with Ste5_pep2^{WT} peptide was made in the absence of kinase (GST-Fus3p) and another without γ^{32}P-ATP. Reaction mixes were incubated at 30ºC and an aliquote was taken for

different time points (10, 30 and 120 minutes). To test for phosphatase Ptc1 competition with Fus3 for the Ste5 phosphosites, Mbp-Ptc1 was included in equal concentration (0.5 μM) and twice (1.0 μM) the concentration of GST-Fus3 in two different assays. Reaction was stopped by adding 6X protein loading buffer (350 mM Tris-Cl (pH 6.8), 10.28% (w/v) SDS, 36% (v/v) glycerol, 0.6 M dithiothreitol, 0.012% (w/v) bromophenol blue. Samples were boiled for 10 minutes and run on 12% SDS-PAGE gels after which the gels were dried, exposed to Amersham Hyperfilm (GE Healthcare) and films were developed on a KODAK M35A X-OMAT processor.

Computational modeling

Assumptions of the model

To explain the switch-like behavior observed in the mating MAPK pathway we constructed a model based on the following assumptions (Fig. 3a and Supplementary Figure 23):

i. Only Ste5, Fus3, and Ptc1 contribute to the switch.
ii. Fus3 phosphorylates identically the 4 phosphosites on Ste5, which surround the Fus3 docking motif (FDM).
iii. In the absence of α-factor, cytosolic Fus3 is not active and cannot phosphorylate Ste5, unless it first binds to the FDM.
iv. The association rate of Fus3 to the FDM on Ste5 is constant, and denoted $f_1^{(K)}$, but its dissociation rate can depend on the number of phosphorylated sites on Ste5, and will be denoted $b_1^{(K)}$ to $b_5^{(K)}$.
v. When Fus3 is bound to the FDM, it is partially active and can bind equally to any of

the unphosphorylated phosphosites of Ste5. The kinase activity of Fus3 obeys a Michaelis-Menten type enzymatic reactions (rates denoted $f_2^{(K)}$, $b_6^{(K)}$ and $k^{(K)}$). We also assume that phosphorylation is distributive. Fus3 needs to dissociate from the FDM after one phosphorylation in order to phosphorylate other sites on Ste5. This assumption is critical to observe zero-order ultrasensitivity.

vi. The amount of Ptc1 available is a function of α-factor. We use a Hill equation with a Hill number of greater than 1 (based on PCA data of Fig. 2e). We assume a small level of Ptc1 even in the absence of α-factor. Mathematically, we have

$$Ptc1 = [Ptc1]_0 + [Ptc1]_{\max} \frac{\alpha^{n_H^{(P)}}}{\alpha^{n_H^{(P)}} + EC_{50}^{(P)n_H^{(P)}}},$$

where $[Ptc1]_0$, $[Ptc1]_{max}$, $n_H^{(P)}$, and $EC_{50}^{(P)}$ are all parameters we fit and α specifies the level of α-factor.

vii. Ptc1 like Fus3 must be first recruited to Ste5 before it can dephosphorylate any phosphosites (rates denoted $f_1^{(P)}$ and $b_1^{(P)}$).

viii. Ptc1 can bind equally to any of the phosphorylated phosphosites of Ste5. Its phosphatase activity obeys a Michaelis-Menten type enzymatic reactions (rates denoted $f_2^{(K)}$, $b_2^{(P)}$ and $k^{(P)}$). We assume that dephosphorylation is also distributive.

ix. At saturating concentrations of α-factor, a small fraction of fully active cytosolic Fus3 called $Fus3_{active}$ can phosphorylate Ste5 without binding to the FDM. The level of active Fus3 is related to α-factor through a Hill function:

$$Fus3_{active} = [Fus3_{active}]_{\max} \frac{\alpha^{n_H^{(K)}}}{\alpha^{n_H^{(K)}} + EC_{50}^{(K)n_H^{(K)}}},$$

where $[Fus3_{active}]_{max}$, $n_H^{(K)}$, and $EC_{50}^{(K)}$ are all parameters that we fit. This

assumption is only necessary to explain the slight increase in the levels of the Ste5-Fus3 complex at high α-factor and it is not essential for the switch.

x. The PCA signal we measure for the Fus3-Ste5 complex reflects the total amount of Fus3 interacting with Ste5 either through the FDM, the phosphosites, or both. Equally, the PCA signal for the Ptc1-Ste5 complex reflects the total amount of Ptc1 interacting with Ste5 either through the Ptc1 binding site, the phosphosites, or both.

Generating sufficient ultrasensitivity

We constructed and tested two different versions of the model. The first assumes that Fus3 or Ptc1 cannot dissociate from their docking motifs when acting at the phosphosites (Fig. 3a and Supplementary Figure 23a). Although this model can produce sharp responses, it cannot explain all the Ste5 mutant data. The second model assumes that the enzymes can dissociate from their docking motifs while acting on the phosphosites (Supplementary Figure 23b). The model of Supplementary Figure 23b fits the data more accurately, although it has two extra parameters ($f_3^{(K)}$ and $f_3^{(P)}$). For clarity, we have shown the first model in Supplementary Figure 23a, but we carry out all our fits with the model of Supplementary Figure 23b. Both models produce sharp responses through a combination of zero-order ultrasensitivity and steric hinderance.

Ultrasensitivity does not occur if the enzymes remain sequestered to the substrate after modification[37]. A distributive enzyme dissociates from the substrate after each modification and needs to be rebound for further modifications. A distributive kinase or phosphatase acting on a substrate with multiple phosphorylation sites can generate ultrasensitive behavior because the rate at which product is formed is determined not just

by the concentration of available enzyme, but by the available concentration raised to a power because the substrate "sees" the concentration of the enzyme once for each enzymatic reaction that occurs[16,38]. In our model a distributive mechanism alone produces a Hill coefficient of about 3 and is not enough to explain the sharp switch. The model of Supplementary Figure 23a assumes distributivity by allowing the enzymes to dissociate from the substrate after modification. The model of Supplementary Figure 23b is more flexible and can accommodate either processive or distributive mechanisms. However, the parameter fit to the data resulted in parameter values that resemble a distributive mechanism.

To understand the roles of steric hinderance and the zero-order mechanism, we tested two modifications of the model in Supplementary Figure 25. If we remove two-stage binding, we will lose enzyme saturation so the switch only works through steric hinderance. This model produces less sharp and less robust switches (Supplementary Figure 25b). The second modification is to keep two-stage binding, but make the affinity of Fus3 to the Ste5 docking site independent of phosphorylation state of Ste5 The model then solely works through zero-order ultrasensitivity because this modification prevents steric hinderance. The sharpness of the switch is lower but robustness to changes in concentration of the enzyme and substrate does not change (Supplementary Figure 25c). Robustness is therefore a property of the two-stage zero-order mechanism. Finally, if we assume Fus3 and Ptc1 bind simultaneously to Ste5, steric hinderance, which relies on competitive binding of Fus3 and Ptc1 to Ste5, would not generate a sharp switch. However, the zero-order mechanism still works.

Another variation of the model that assumes non-identical phosphosites can produce bistability[14,39]. Since the data for the Ste5 mutants in Supplementary Figures 10-12 suggest that all phosphosites have similar effects, however, we worked with a model with identical phosphosites.

Local saturation generates a robust ultrasensitivity

To understand how two-stage binding generates a highly ultrasensitive response that is robust to the ratio of the concentration of the enzymes to the concentration of the substrate Ste5, let us first consider classic zero-order ultrasensitivity with one-stage binding and with Ste5 having only one phosphosite. For ease of explanation, we will discuss the completely symmetric case, with equal concentrations of kinase and phosphatase and with the kinetic rates for the action of the kinase identical to the corresponding rates for the action of the phosphatase. At steady-state then half of all Ste5 molecules will be phosphorylated, and both the kinase and the phosphatase will be saturated if there is a sufficiently high concentration of Ste5. Any increase in the concentration of phosphatase will increase the number of unphosphorylated substrates and therefore maintain the saturation of the kinase. A small increase in the phosphatase concentration therefore generates a large decrease in the concentration of phosphorylated Ste5 because any additional phosphatase has no competition from the kinase. Similarly, for a large increase in the concentration of phosphorylated Ste5 for a small decrease in the concentration of the phosphatase, we require that the phosphatase remains saturated.

Two-stage binding allows local saturation of the enzymes. With two-stage binding, the initial binding of an enzyme to the substrate occurs at a rate independent of the state

of phosphorylation of the substrate because the enzyme binds only to its docking site on the substrate. Once bound, an enzyme can either dissociate or bind to one of the substrate's phosphosites, either unphosphorylated sites for the kinase Fus3 or phosphorylated sites for the phosphatase Ptc1. We say that an enzyme is locally saturated when the probability of an enzyme binding to a phosphosite rather than dissociating from Ste5 is close to unity. This probability is determined by the rate of dissociation of the enzyme from its docking site and the rate of associating with a single phosphosite multiplied by the number of available phosphosites. Therefore increasing the number of phosphosites on Ste5 increases the potential degree of local saturation of the enzymes.

Ultrasensitivity generated through two-stage binding of both enzymes to the substrate is analogous to classic zero-order ultrasensitivity. Consider again the completely symmetric case, but now with two stage-binding and multiple phosphosites on Ste5. For equal concentrations of enzymes, half of these phosphosites on all Ste5 molecules will be phosphorylated. With a sufficient number of phosphorylation sites, both enzymes will therefore be locally saturated regardless of the ratio of their concentration to the concentration of Ste5 or whether they have their own docking sites on Ste5 or compete for a single docking site. If we increase the concentration of the phosphatase at this steady-state, then the local saturation of the kinase is maintained. More phosphatase will increase the number of unphosphorylated phosphosites on Ste5 increasing the probability that a kinase once bound to Ste5 will bind a phosphosite rather than dissociate. If the kinase and phosphatase have their own docking sites on Ste5 then the rate of binding of the kinase to Ste5 will remain unchanged; if they compete for the same docking site, the rate of binding of the kinase will decrease. Analogous to classic

zero-order ultrasensivity, any small increase in the concentration of the phosphatase will therefore be unopposed by the kinase and generate a large decrease in the level of phosphorylation of Ste5. We emphasize that this ultrasensitive decrease will occur regardless of the ratio of the concentration of the enzymes to the substrate providing the enzymes are locally saturated. For example, ultrasensitivity will be undermined with just one phosphorylation site on Ste5 or with processive enzymes because then increasing the concentration of phosphatase will increase the concentration of completely unphosphorylated substrates and so allow the total rate of phosphorylation to also increase. With many phosphosites on Ste5 and distributive enzymes, however, a phosphatase dephosphorylates at most one phosphosite each time it binds to Ste5, and multiple phosphorylated phosphosites on Ste5 are maintained. All kinases consequently remain locally saturated when bound to a substrate, and the rate of phosphorylation does not increase.

Mathematical details

Our model has 27 parameters **(Supplementary Table 3)**. For the kinetic rates in Supplementary Figure 23b, the concentrations of the enzymes Fus3 and Ptc1 and of Ste5, we assume that;

i. The concentration of Ste5 is 0.052 μM and Fus3 is 0.197 μM by averaging published data[40].
ii. The level of the PCA signal for the Fus3-Ste5 interaction in wild type cells in the absence of pheromone (F) corresponds to 20% of the Ste5 concentration (~0.01 μM) from Maeder *et al.*[40]. This choice scales the values of the dissociation

constants we fit.

iii. We fit all the other parameters and kinetic rates to the Fus3-Ste5 (Fig. 2a) and the Ptc1-Ste5 (Fig. 2e) PCA data of the dose-response to α-factor and to the PCA data for the Fus3-Ste5 interaction with the pseudo-phosphorylated mutants of Ste5 (Fig. 2d).

The model was constructed using the *Facile* network compiler[28] with Allosteric Network Compiler a rule-based modeling scheme, courtesy of Julien Ollivier, to generate a description of the model as a set of differential equations. We integrated the model in Matlab (The Mathworks, Nattick, Massachusetts). To fit the data, we optimized the parameters using an efficient Markov chain Monte Carlo method[29], which uses an adaptive Metropolis sampler and delayed rejection.

We give the differential equations for the model below. Here $Ste5^n$ denotes Ste5 with n phosphorylated sites where n is an integer between 0 and 4. We have 3 distinct forms of Ste5-Fus3 complexes: Fus3_$Ste5^n$_0 denotes a complex where Fus3 is only bound to the FDM, shown by (0) (Supplementary Figure 23b); Fus3_$Ste5^n$_1 denotes a complex where Fus3 is bound to the FDM and to a phosphosite, shown by (1); and Fus3_$Ste5^n$_2 denotes a complex where Fus3 is bound only to a phosphosite, shown by (2). Similarly, Ste5-Ptc1 complexes have the same three forms denoted by Ptc1_$Ste5^n$_0, Ptc1_$Ste5^n$_1 and Ptc1_$Ste5^n$_2 (Supplementary Figure 23b).

The concentration of each species in Supplementary Figure 23b changes with time and is described by a differential equation:

$$\frac{dFus3}{dt} = \sum_{n=0}^{4} b_n^{(K)}.Fus3\_Ste5^n\_0 - f_1^{(K)}.Fus3.\sum_{n=0}^{4} Ste5^n + \sum_{n=0}^{3} k^{(K)}.Fus3\_Ste5^n\_2 + \sum_{n=0}^{3} b_6^{(K)}.Fus3\_Ste5^n\_2.$$

$$\frac{dPtc1}{dt} = \sum_{n=0}^{4} b_1^{(P)}.Ptc1\_Ste5^n\_0 - f_1^{(P)}.Ptc1.\sum_{n=0}^{4} Ste5^n + \sum_{n=1}^{4} k^{(P)}.Ptc1\_Ste5^n\_2 + \sum_{n=1}^{4} b_2^{(P)}.Ptc1\_Ste5^n\_2.$$

For n= 0 to 4, we have (For n=0 and n=4, we ignore any terms that result in $Ste5^{-1}$ and $Ste5^5$.):

$$\frac{dSte5^n}{dt} = b_n^{(K)}.Fus3\_Ste5^n\_0 - f_1^{(K)}.Fus3.Ste5^n + b_1^{(P)}.Ptc1\_Ste5^n\_0 - f_1^{(P)}.Ptc1.Ste5^n + k^{(K)}.Fus3\_Ste5^{n-1}\_2 + k^{(P)}.Ptc1\_Ste5^{n+1}\_2 + b_6^{(K)}.Fus3\_Ste5^n\_2 + b_2^{(P)}.Ptc1\_Ste5^n\_2.$$

$$\frac{dFus3\_Ste5^n\_0}{dt} = f_1^{(K)}.Fus3.Ste5^n - b_n^{(K)}.Fus3\_Ste5^n - (4-n).f_2^{(K)}.Fus3\_Ste5^n\_0 + b_6^{(K)}.Fus3\_Ste5^n\_1 + k^{(K)}.Fus3\_Ste5^{n-1}\_1.$$

$$\frac{dPtc1\_Ste5^n\_0}{dt} = f_1^{(P)}.Ptc1.Ste5^n - b_1^{(P)}.Ptc1\_Ste5^n - n.f_2^{(P)}.Ptc1\_Ste5^n\_0 + b_2^{(P)}.Ptc1\_Ste5^n\_1 + k^{(P)}.Ptc1\_Ste5^{n+1}\_1.$$

For n=0 to 3, we have:

$$\frac{dFus3\_Ste5^n\_1}{dt} = (4-n).f_2^{(K)}.Fus3\_Ste5^n\_0 - b_6^{(K)}.Fus3\_Ste5^n\_1 - k^{(K)}.Fus3\_Ste5^n\_1 - b_n^{(K)}.Fus3\_Ste5^n\_1 + f_3^{(K)}.Fus3\_Ste5^n\_2.$$

$$\frac{dFus3\_Ste5^n\_2}{dt} = b_n^{(K)}.Fus3\_Ste5^n\_1 - k^{(P)}.Fus3\_Ste5^n\_2 - b_6^{(K)}.Fus3\_Ste5^n\_2 - f_3^{(K)}.Fus3\_Ste5^n\_2.$$

For n=1 to 4, we have:

$$\frac{dPtc1\_Ste5^n\_1}{dt} = n.f_2^{(P)}.Ptc1\_Ste5^n\_0 - b_2^{(P)}.Ptc1\_Ste5^n\_1 - k^{(P)}.Ptc1\_Ste5^n\_1 - b_1^{(P)}.Ptc1\_Ste5^n\_1 + f_3^{(P)}.Ptc1\_Ste5^n\_2.$$

$$\frac{dPtc1\_Ste5^n\_2}{dt} = b_1^{(P)}.Ptc1\_Ste5^n\_1 - k^{(P)}.Ptc1\_Ste5^n\_2 - b_2^{(P)}.Ptc1\_Ste5^n\_2 - f_3^{(P)}.Ptc1\_Ste5^n\_2.$$

In total, there are 33 equations. In addition, if we assume some level of $Fus3_{active}$ we have an additional 5 equations:

$$\frac{dFus3_{active}}{dt} = \sum_{n=0}^{4} b_6^{(K)}.Fus3_{active}\_Ste5^n - (4-n).f_4^{(K)}.Fus3_{active}.\sum_{n=0}^{4} Ste5^n + \sum_{n=0}^{3} k^{(K)}.Fus3_{active}\_Ste5^n\_2.$$

For n =0 to 3, we have:

$$\frac{dFus3_{active}\_Ste5^n}{dt} = (n-4).f_4^{(K)}.Fus3_{active}.Ste5^n - b_6^{(K)}.Fus3_{active}\_Ste5^n - k^{(K)}.Fus3_{active}\_Ste5^n.$$

We also need to add terms to the $Ste5^n$ equations to describe the phosphorylation carried out by $Fus3_{active}$.

We investigated the sensitivity of the switch to variation in the parameters of the model. Changes in concentrations of Ste5, Fus3, and Ptc1 can all influence the EC_{50} and n_H (Supplementary Figure 26). We observe, however, a high Hill number in the population data (Figure 2a), which suggests that the EC_{50} and n_H of the switch in single cells should not be very variable between cells. This robust behavior could result from correlated fluctuations in the concentrations of Fus3, Ste5 and Ptc1, as suggested recently in other systems[41,42].

Figure 3c is generated using a classic model of zero-order ultrasensitivity with only one phosphosite. The kinetic parameters for the Michaelis-Menten reactions we use are:

$f^{(K)} = f^{(P)} = 500\ nM^{-1}s^{-1}$,

$b^{(K)} = b^{(P)} = 1\ s^{-1}$,

$k^{(K)} = k^{(P)} = 1\ s^{-1}$.

Supplementary Figures

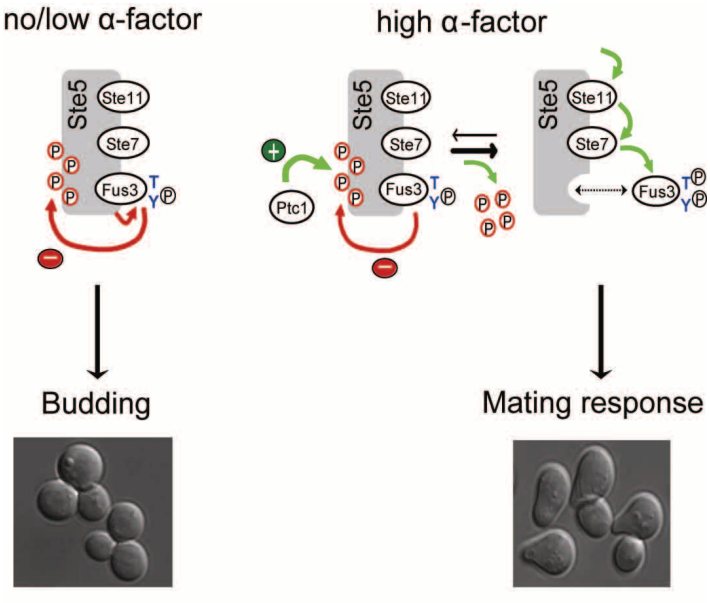

Supplementary Figure 1 Schematic for the direct control of mating decision by the Ste5 scaffold

Although essential for mating, Fus3 through binding to Ste5 is initially inhibitory. Multisite phosphorylation of Ste5 by partially active Fus3 increases the association of Fus3 with Ste5. In the absence of a mate or when two potential mates are far from each other, these phosphorylations of Ste5 prevent release and full activation of Fus3 and hence shmooing. High α-factor concentrations indicating the presence of a suitable mate induces dephosphorylation of Ste5 and allows Fus3 to become fully activated and induce shmooing and eventually mating.

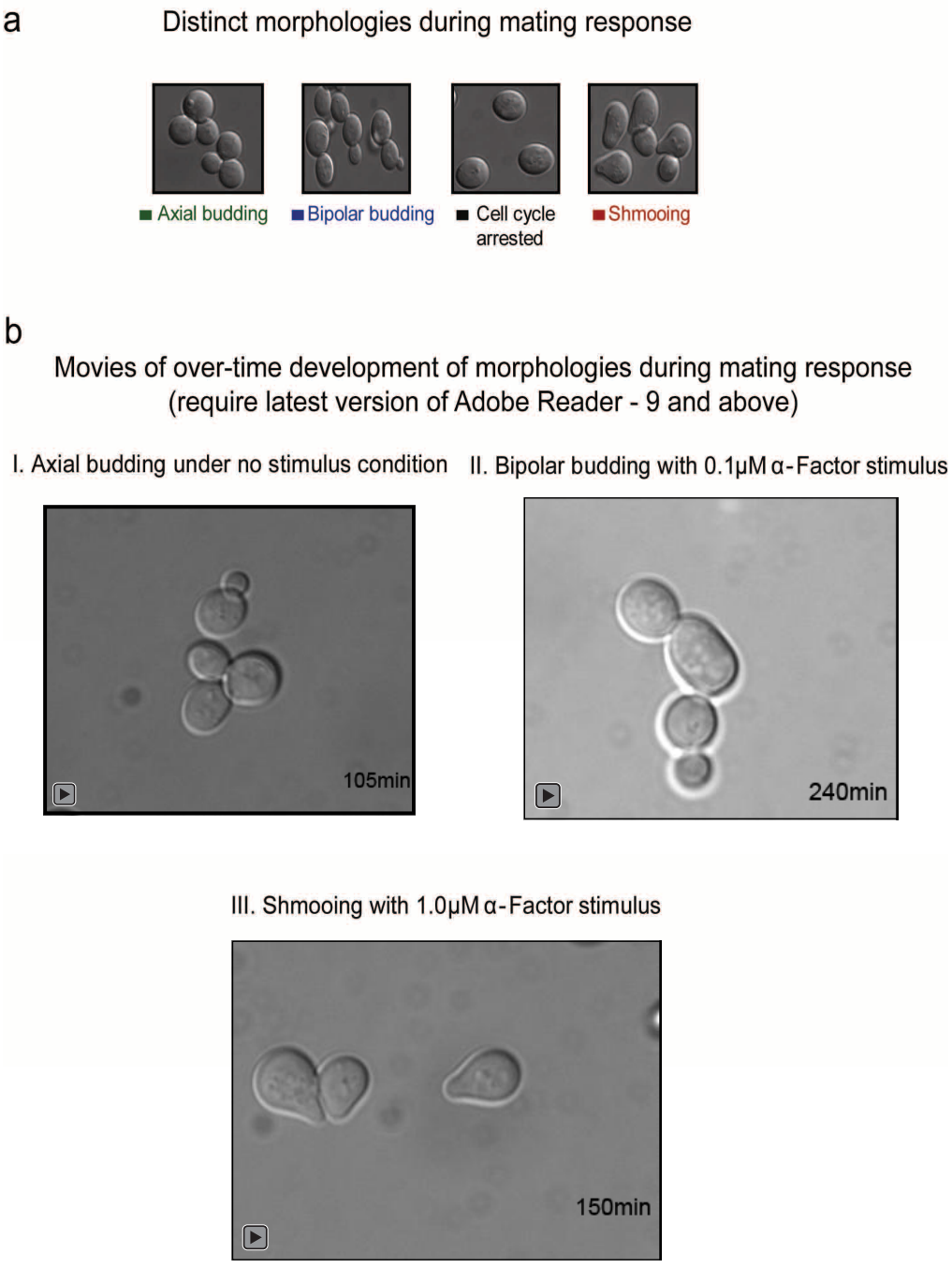

Supplementary Figure 2 Different morphological phenotypes during mating response

(a) Different morphological states of yeast during mating response: Axial budding, bipolar budding, cell cycle arrested and shmooing.

(b) Movies to show the development over-time of axial budding (I), bipolar budding (II) and shmooing (III) morphologies during the pheromone response. To view the movies, please click on the respective images. The latest version of Adobe Reader (9 and above) is needed to view the movies directly in this pdf document.

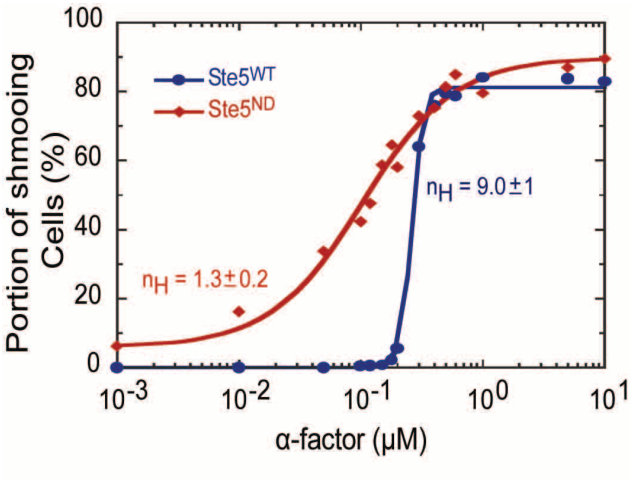

Supplementary Figure 3 Fus3 interaction with Ste5 is essential for the switch-like shmooing response

α-factor-dependent changes in the fraction of shmooing cells in *ste5*Δ strain expressing either $Ste5^{WT}$ (blue circles) or $Ste5^{ND}$ (red diamonds). Assuming the final shmooing response is driven by underlying molecular events, the data for shmooing cells from Figure 1b & c were fit to a Hill function. The Hill coefficients [18] were calculated from the fit.

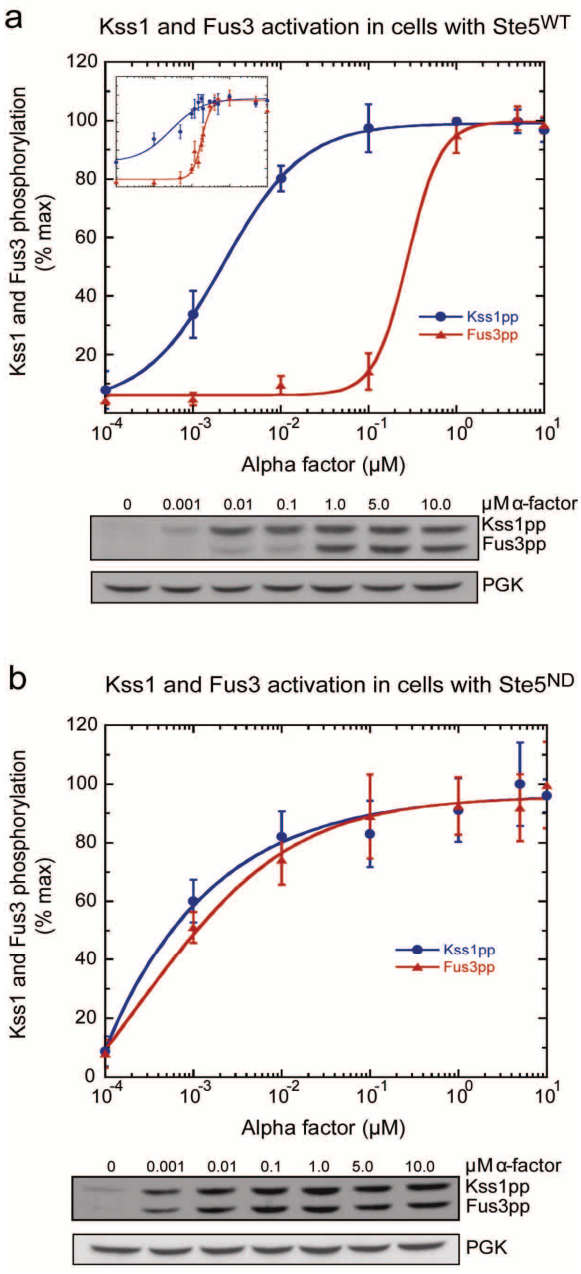

Supplementary Figure 4 MAP kinase Kss1 and Fus3 activation levels during mating response

The activation levels of MAPKs (Fus3 and Kss1) measured in *ste5*Δ cells expressing $Ste5^{WT}$ (a) and $Ste5^{ND}$ (b) after stimulating with the indicated concentration of α-factor. Fully active MAPK levels (dually phosphorylated) were detected by western blotting using anti-phospho MAPK antibody. Inset curves in (a) shows similar activation profiles for Fus3 and Kss1 when measured with many more concentrations in the dynamic range of response. Error bars indicate the standard errors of the mean from three experiments. Phosphoglycerate kinase (PGK) expression level was used as loading controls.

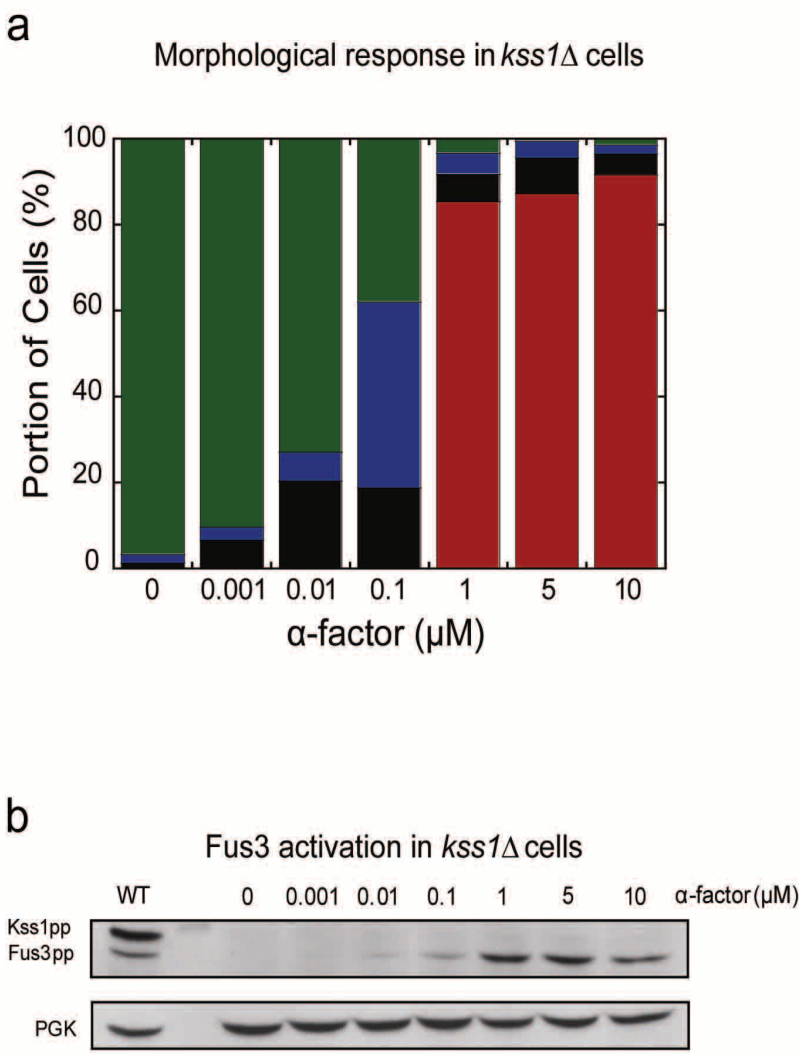

Supplementary Figure 5 Mating response in *kss1*Δ cells

(a) Mating response in *kss1*Δ cells. In a dose response to α-factor, cells lacking Kss1 respond similar to wild type cells with no detectable difference in shmooing ability.

(b) Active Fus3pp levels detected by Western blotting using anti-phospho MAPK antibody. Kss1 does not interfere with the switch-like activation of Fus3pp in an α-factor dose response.

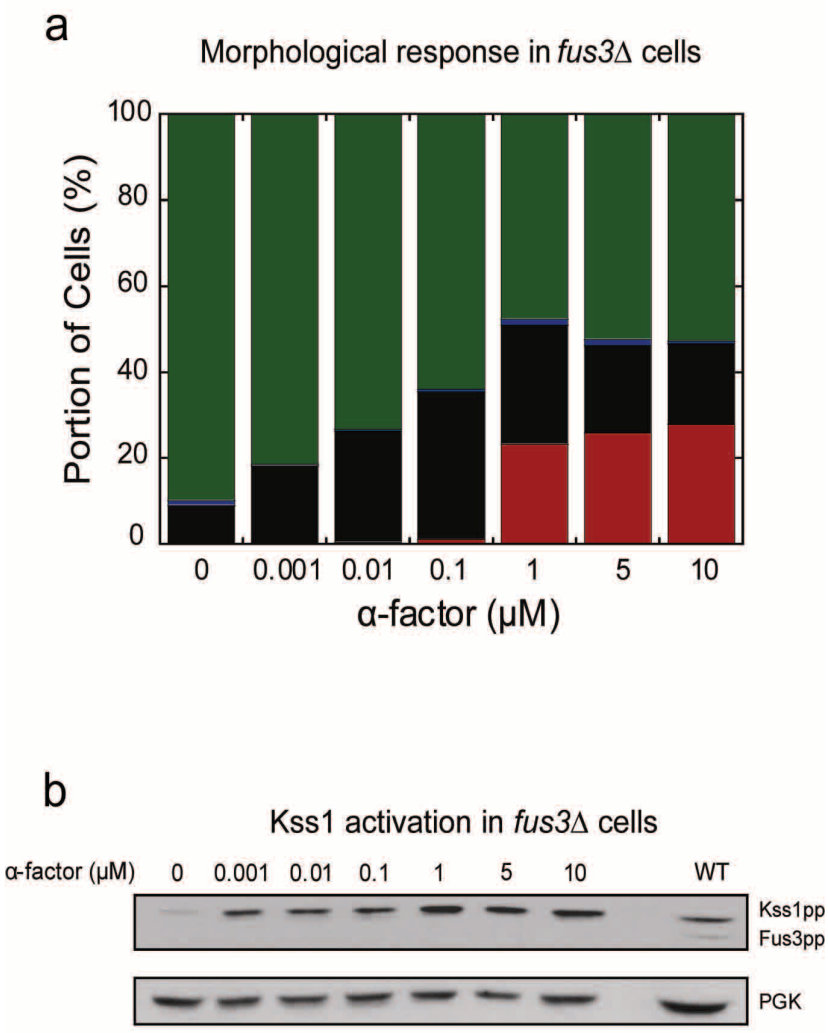

Supplementary Figure 6 Mating response in *fus3*Δ cells

(a) Mating response in *fus3*Δ cells. In a dose response to α-factor, cells lacking Fus3 have a severely diminished shmooing ability. Bipolar budding is lost and very minimal shmooing was observed. The homologue of Fus3 MAPK, Kss1, which is also activated during the pheromone response, partially compensates for the role of Fus3.

(b) Active Kss1pp levels detected by Western blotting using anti-phospho MAPK antibody. Kss1pp exhibits a linear rather than a switch-like activation. Thus, Fus3 is essential for the mating response along with the switch-like differentiation of shmooing cells.

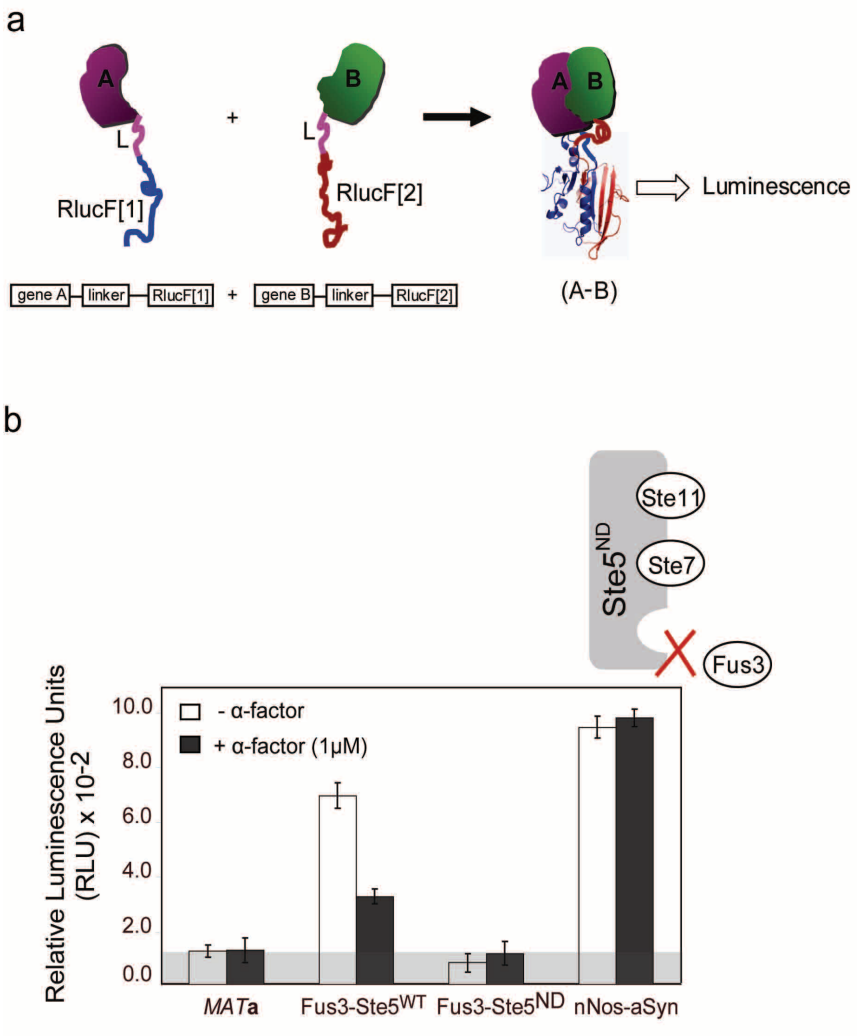

Supplementary Figure 7 Renilla luciferase PCA (Rluc PCA) to measure the dynamics of protein-protein interactions

(a) Schematic model with hypothetical proteins to show the PCA strategy. PCA fragments F[1] and F[2] (in this study Rluc F[1] and Rluc F[2]) are fused to the C-terminus of the proteins of interest A and B respectively and preceded by a 10 amino acid flexible linker ($(GGGGS)_2$). Only when the two proteins interact do the fragments of the PCA reporter (e. g. Renilla luciferase) fold into a fully functional enzyme. The activity of the functional enzyme is measured as the readout for a direct protein-protein interaction between A and B. For Rluc PCA, bioluminescence is measured using a luminometer as a function of protein-protein interaction.

(b) Specificity of Rluc PCA for the Fus3 and Ste5 interaction. Using Rluc PCA, a specific interaction between Fus3 and Ste5 can be measured along with its dynamics under α-factor treated conditions. With a mutant of Ste5 ($Ste5^{ND}$)[9] that is known to disrupt its interaction with Fus3, the PCA signal reduces to background. Two PDZ domains that are known to form heterodimers (nNOS and aSyn)[32] are used as a positive control for Rluc PCA and as a negative control for the dynamics induced as a function of α-factor.

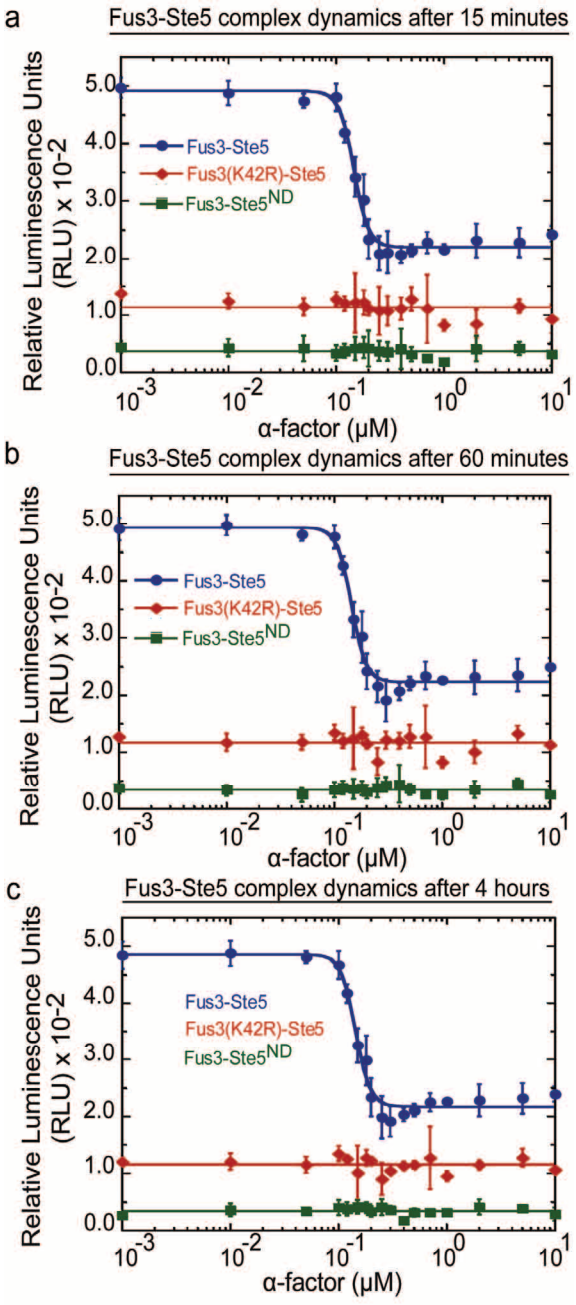

Supplementary Figure 8 Steady state levels of the Fus3-Ste5 complex at different time points during the mating response

The steady-state levels of the Fus3-Ste5 complex at 15 minutes (a), 60 minutes (b) and 4 hours (c) after treatment with the indicated concentration of α-factor in a dose response. Errors indicate the standard error of the mean from three experiments.

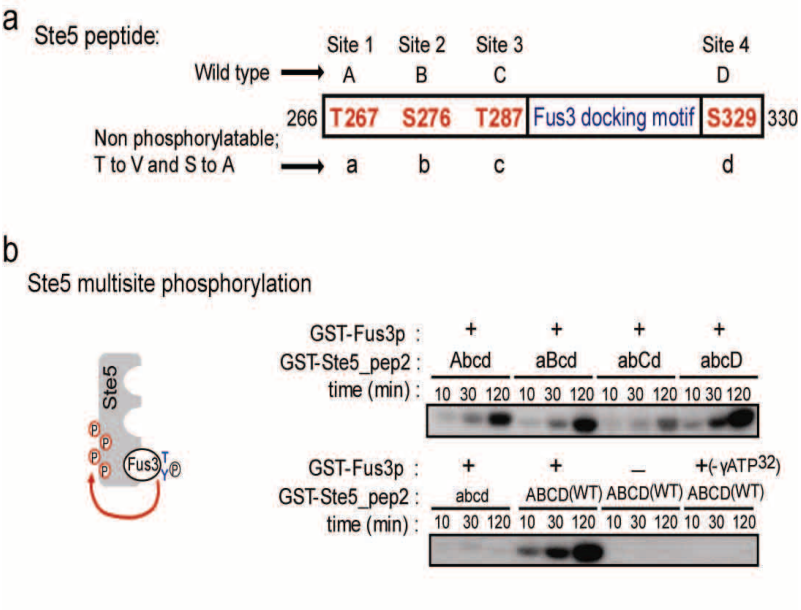

Supplementary Figure 9 Partially active Fus3 phosphorylates all four Ste5 phosphosites in an *in-vitro* kinase assay.

(a) A map of the Ste5 peptide (residues 266 to 330) showing the four MAPK phosphorylation sites and their mutations. Phosphosites 1, 2, 3 and 4 are *wildtype* (A, B, C, or D) or non-phosphorylatable mutants (a, b, c, or d) with either threonine (T) to valine (V) or serine (S) to alanine (A).

(b) Schematic: Ste5-bound, partially activated Fus3 phosphorylates all four phosphosites. Autoradiography of phosphorylation on individual phosphosites of Ste5 using the indicated form of GST-Ste5_pep2 (residues 214 to 334) in the presence or absence of GST-Fus3p and γ^{32}P-ATP.

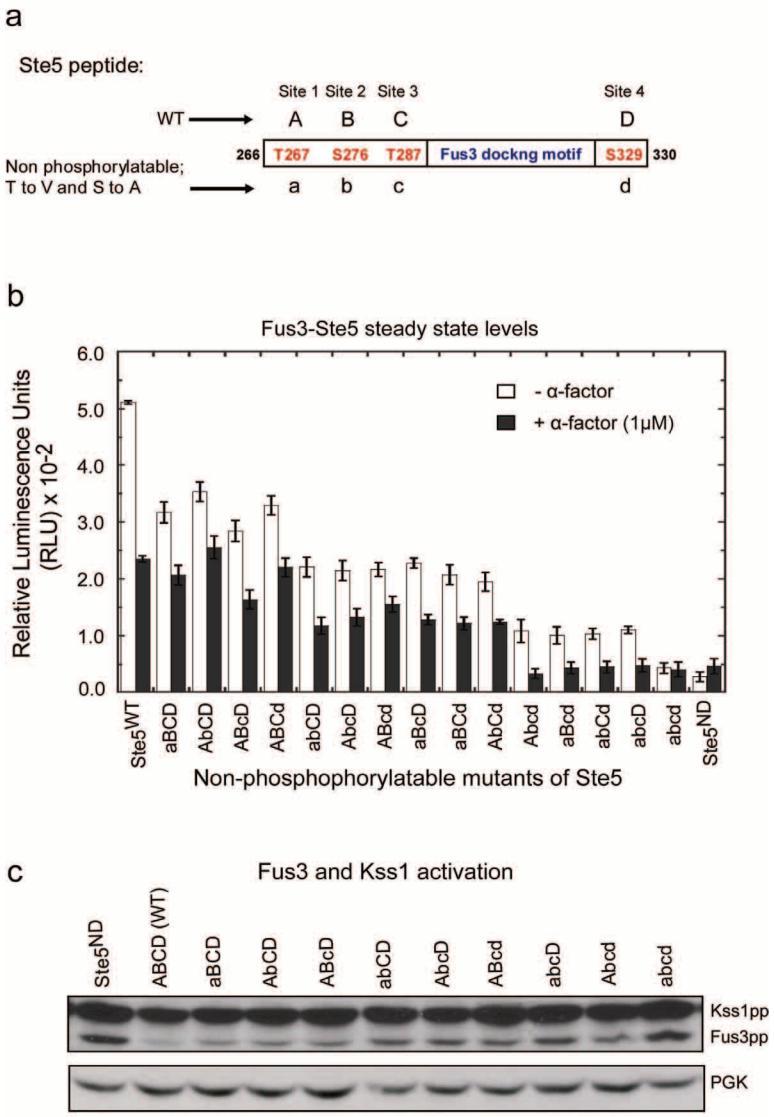

Supplementary Figure 10 Non-phospho mutants of Ste5 and their effect on the Fus3-Ste5 steady-state

(a) A map of a Ste5 peptide (residues 266 to 330) showing the location of the consensus MAPK phosphorylation site (S/T-P) mutations. Phosphosites 1, 2, 3 and 4 are labeled as follows: wild type (WT): Capital A, B, C and D; non-phosphorylatable form: small a, b, c and d. To generate these mutations all threonines (T) were mutated to valine (V) and serines (S) to alanine (A).

(b) The effect of non-phosphorylatable mutations, either singly or in combinations of two, three or all four sites on the steady-state levels of the Fus3-Ste5 complex under non-treated and α-factor treated conditions.

(c) The activity levels of the MAPKs Fus3 and Kss1 detected by Western blotting with the non-phosphorylatable mutants. Fus3 activation increase with an increase in the number of non-phosphorylatable sites while there is no change in the activation of Kss1. Cells were treated with 1 μM of α-factor for 15 minutes.

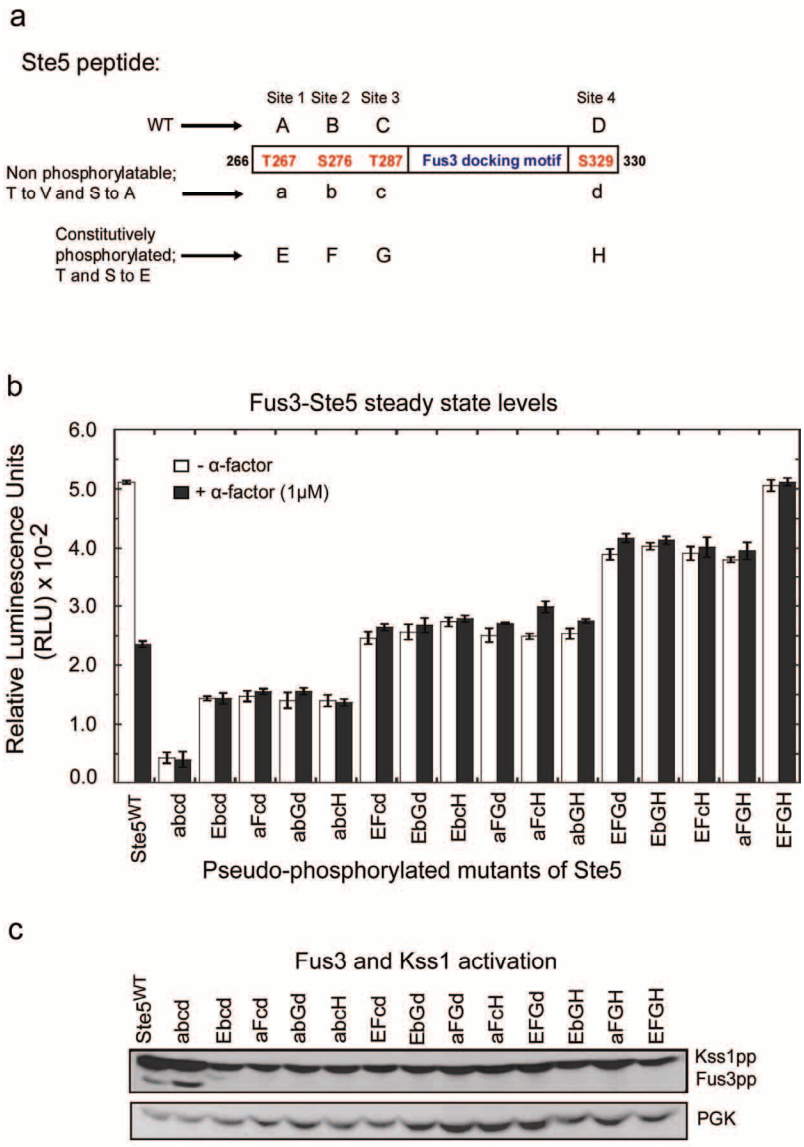

Supplementary Figure 11 Constitutively active phosphosite mutants of Ste5 and their effect on the steady-state levels of the Fus3-Ste5 complex

(a) A map of a Ste5 peptide showing the location of the consensus MAPK phosphorylation site (S/T-P) mutations. Phosphosites 1, 2, 3 and 4 are labeled as follows: wild type (WT): capital A, B, C and D; non-phosphorylatable form: small a, b, c and d; constitutively phosphorylated form: capital E, F, G and H. To generate constitutively active phosphosites both threonines and serines were mutated to glutamic acid (E).

(b) The effect of constitutively phosphorylated mutations, either singly or in combinations of two, three or all four sites on the steady-state levels of the Fus3-Ste5 complex under non-treated and α-factor treated conditions.

(c) The activation levels of the MAPKs Fus3 and Kss1 detected by Western blotting with the indicated pseudo-phosphorylation mutants. Fus3 activation is completely prevented if there is a single pseudo-phosphorylated site. While there is no change in the activation levels of Kss1.

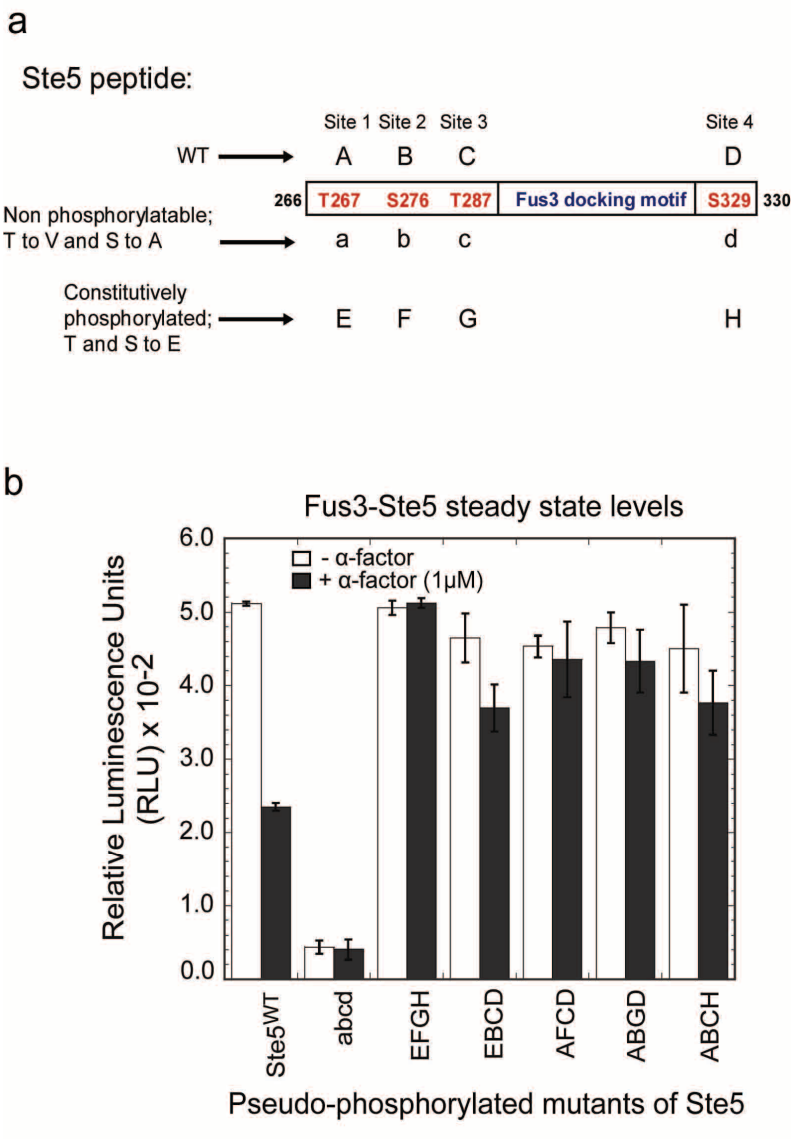

Supplementary Figure 12 Constitutively active phosphosite mutants of Ste5 on single sites and their effect on the steady-state levels of the Fus3-Ste5 complex

(a) A map of a Ste5 peptide showing the location of the consensus MAPK phosphorylation site (S/T-P) mutations.

(b) The effect of the constitutively pseudo-phosphorylated mutations at single sites on Ste5 on the steady-state levels of the Fus3-Ste5 complex under non-treated and α-factor treated conditions.

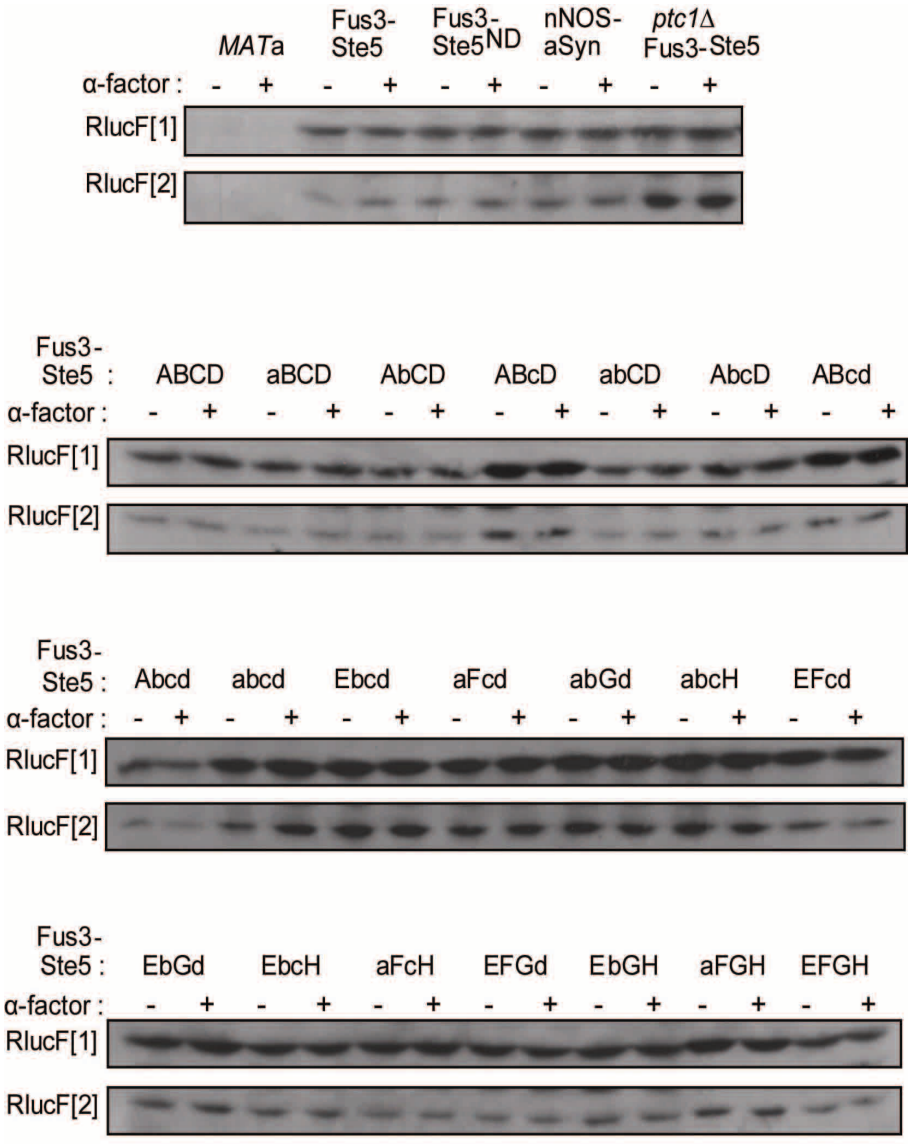

Supplementary Figure 13 Protein expression of genes fused with Rluc PCA fragments

Normal expression levels of genes fused with Rluc fragments including the variants of Ste5 were checked using the specific antibodies for Rluc F[1] and Rluc F[2]. Expression levels were checked without and with α-factor treatment (1 μM) as indicated. As seen, the fusion of Rluc fragments does not interfere with the normal expression levels of the genes modified in the study.

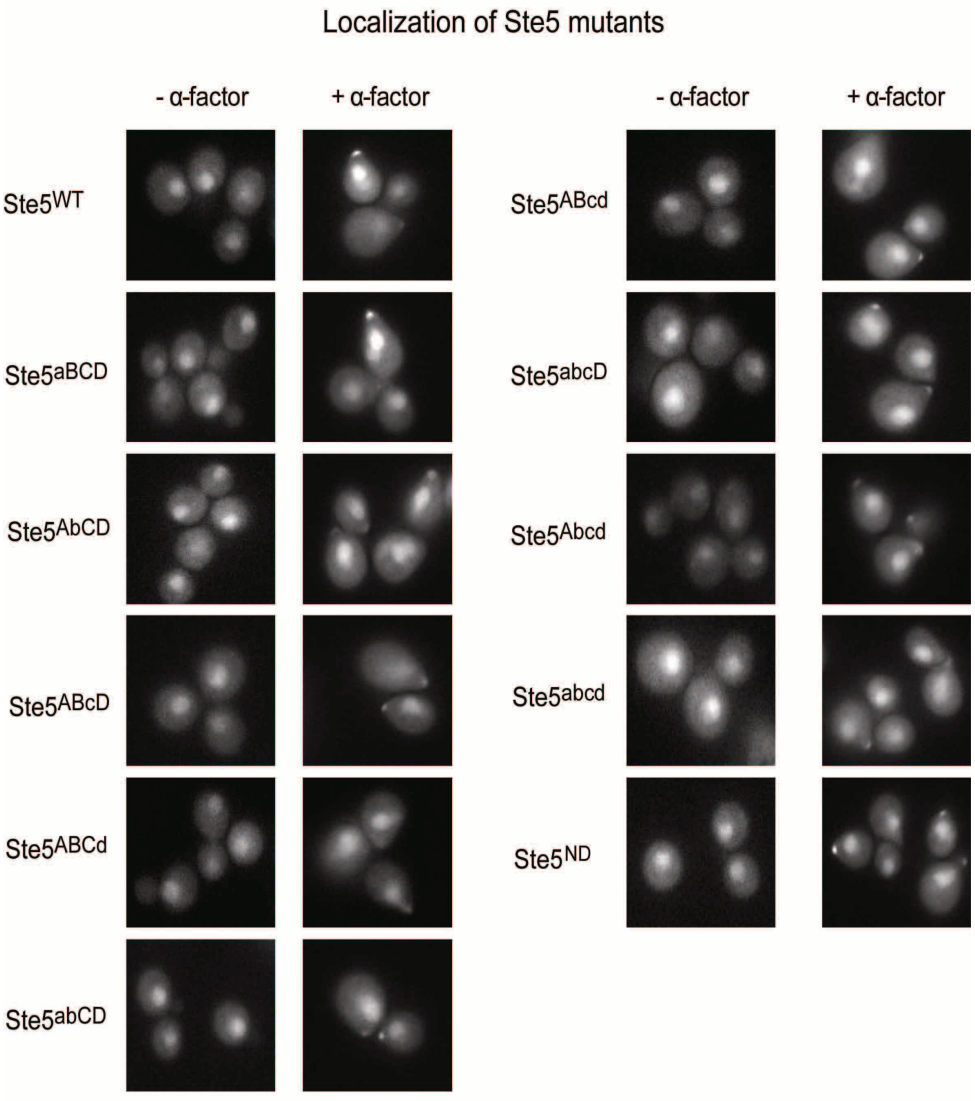

Supplementary Figure 14 Cellular location of the variants of Ste5 with phosphosite mutations

Fluorescence microscopy images showing the location of the indicated form of Ste5 under non-treated and α-factor treated (1μM) conditions. Consistent with previously work, variants of Ste5 are predominantly in the nucleus in the absence of stimulus and localize to 'shmoo tip' in the presence of α-factor. Thus, the phosphosite mutations do not seem to affect the normal localization and expression of Ste5, but selectively regulate its interaction with Fus3.

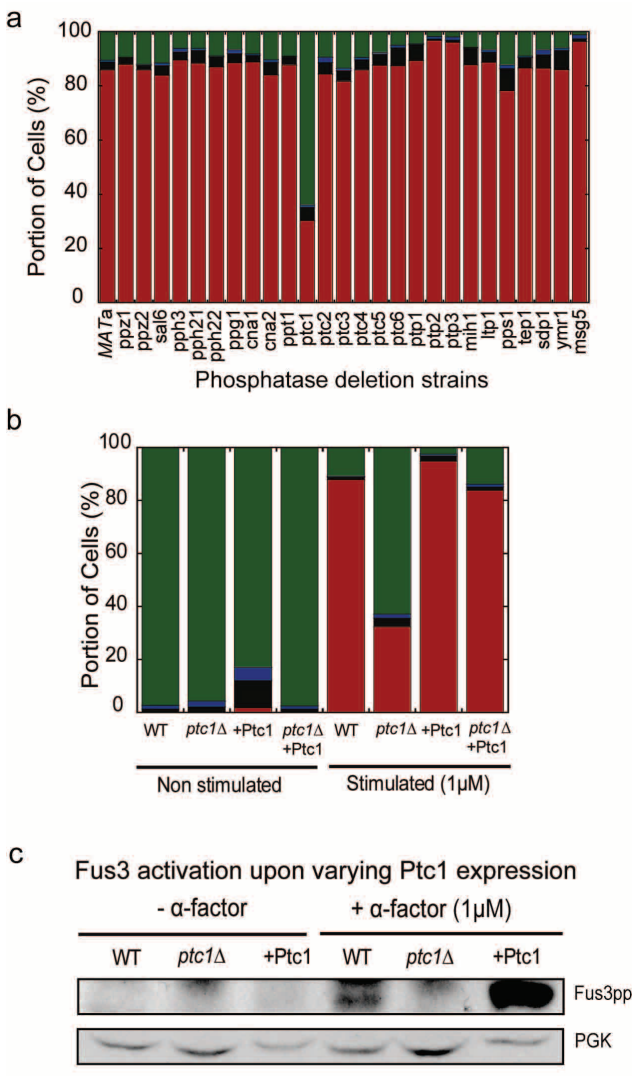

Supplementary Figure 15 Serine/threonine phosphatase Ptc1 is required for the mating response

(a) Morphological responses in a collection of *MAT***a** strains deleted individually for one of the 26 phosphatase genes in yeast in comparison to *wildtype* (*MAT***a**) cells.

(b) The fraction of cells with different phenotypes in strains with *wildtype* (WT), knockout (*ptc1*Δ), over-expression of Ptc1 (+Ptc1) and *ptc1*Δ with plasmid-borne Ptc1 (*ptc1*Δ + Ptc1). In +Ptc1 and *ptc1*Δ + Ptc1 strains, Ptc1 was constitutively expressed from a plasmid under the control of the *ADH* promoter. Cells were stimulated with 1 μM α-factor for 3 to 4 hours. Phenotypes are color-coded: axial budding (green), bipolar budding (blue), cell cycle arrested (black) and shmooing (red).

(c) Fus3pp levels detected using anti-phospho MAPK antibody in cells lacking Ptc1 (*ptc1*Δ) and over-expressing Ptc1 (+*PTC1*) in comparison to wild type (WT) *MAT***a** under non-treated and α-factor treated conditions. To over-express Ptc1, it was expressed constitutively under the ADH promoter from a plasmid (pMM60). The absence of Ptc1 reduced the activation of Fus3 and its over-expression substantially increased the levels of active Fus3.

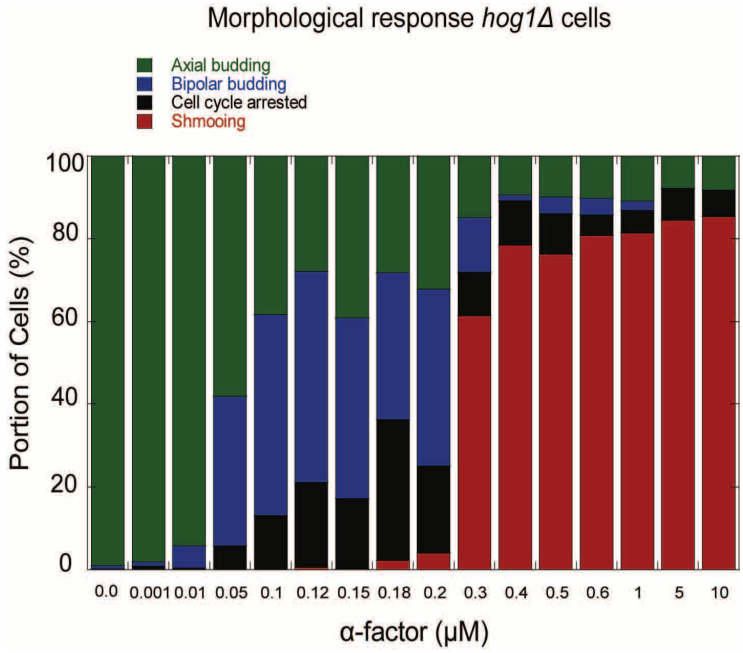

Supplementary Figure 16 The shmooing response is insensitive to the deletion of Hog1

Histograms showing the portion of different morphologies observed with increasing concentrations of α-factor in *hog1Δ* cells. Results show that the response with *hog1Δ* cells is identical to *wild type* cells (Figure 1b). Although the fraction of bipolar budding and cell cycle arrested cells are slightly reduced, the switch-like dose response of shmoo formation to pheromone is insensitive to the deletion of Hog1.

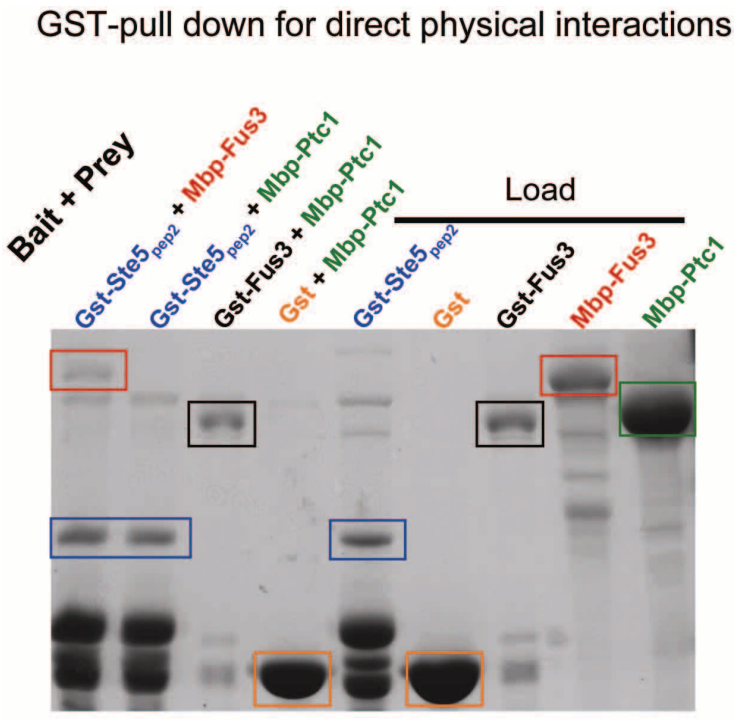

Supplementary Figure 17 A physical interaction of Ptc1 with Fus3 and Ste5

In vitro binding experiment using GST-pull down to test for the interaction of Ptc1 with Fus3 and Ste5_pep2 (Ste5). The indicated proteins are used as bait or prey in the GST-pull downs. Bands in color coded boxes correspond to the respective color coded proteins while the rest of the bands are mostly degradation products or contaminants during purifications. The known interaction of Fus3 with Ste5_pep2 is detected (lane 1). In agreement with its α-factor stimulus dependant recruitment and its interaction with the phosphosites on Ste5 (Figure 2f and Supplementary Figure 16), Ptc1 is observed not to interact with non-phosphorylated Ste5_pep2 (lane 2). Ptc1 was also found to not interact with Fus3 (lane 3). GST alone was used as negative control (lane 4). Lanes 5 to 9 indicate the loadings.

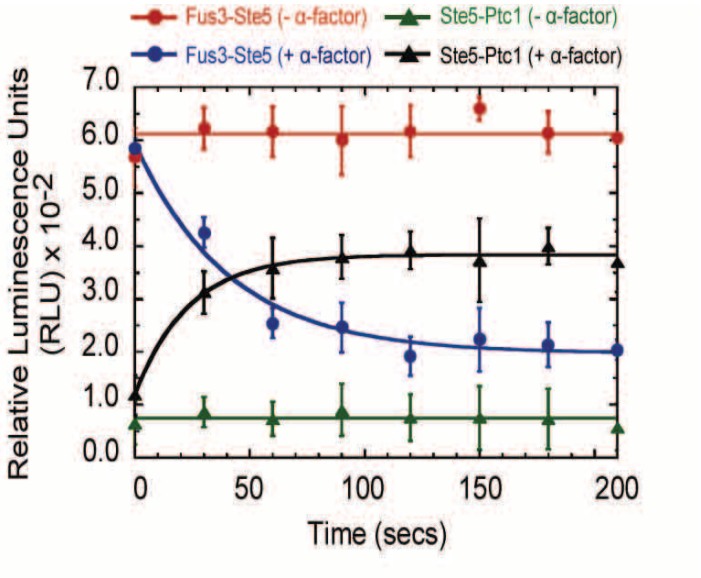

Supplementary Figure 18 Fus3 dissociates from Ste5 simultaneous to the association of Ptc1 with Ste5

Real-time kinetics for the Fus3-Ste5 and Ste5-Ptc1 interactions using Rluc PCA. Data were fit to a single exponential giving effective rates of $0.04s^{-1}$ for Ste5-Ptc1 (R^2=0.99) and $0.02s^{-1}$ for Fus3-Ste5 (R^2=0.97).

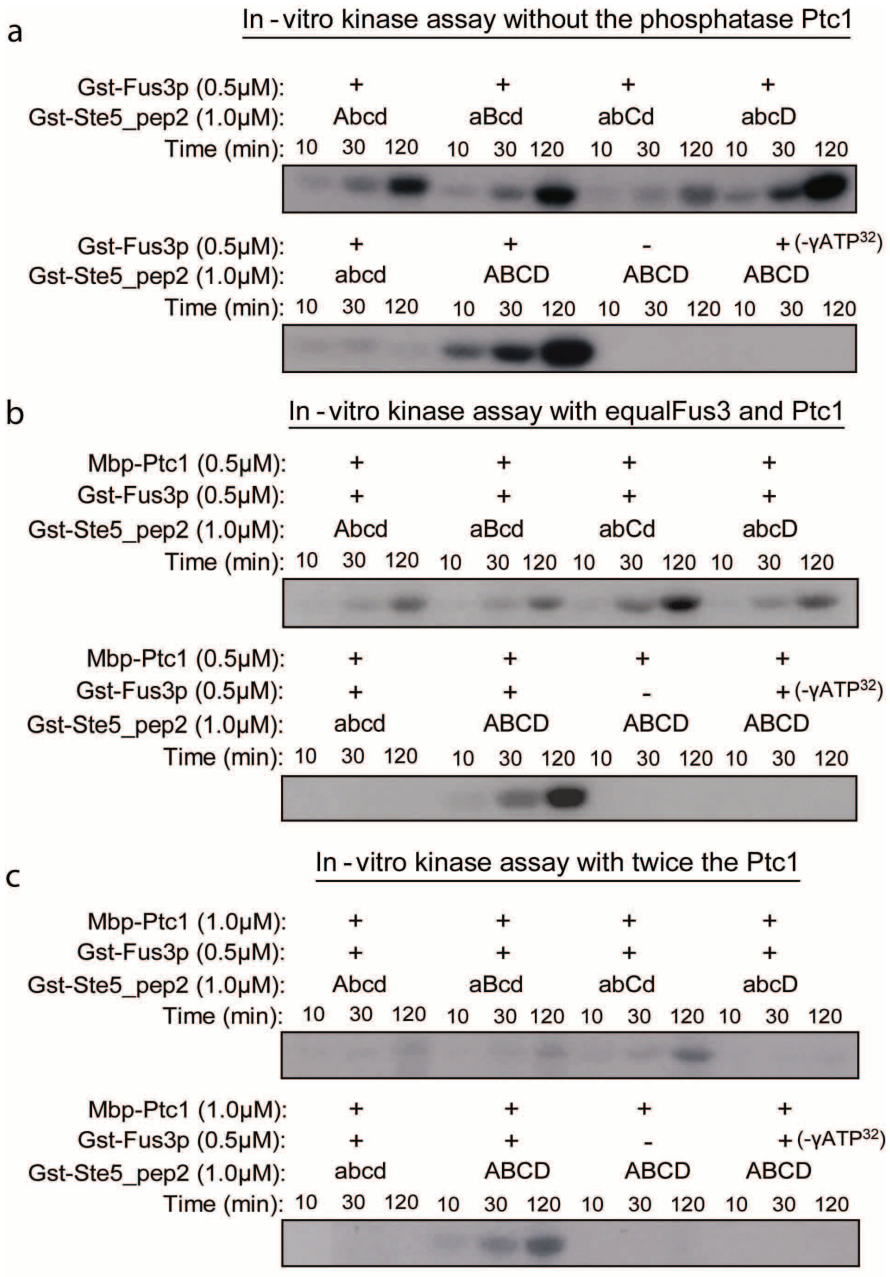

Supplementary Figure 19 Ptc1 is capable of dephosphorylating the Ste5 phosphosites by competing with Fus3

Blots from an *in vitro* kinase assay without the phosphatase Ptc1 (a), with equal Fus3 and Ptc1 (b) and with twice the amount of Ptc1 to Fus3 (c). Phosphorylation levels decrease with an increase in Ptc1 concentration. In conclusion, Ptc1 can interact with and dephosphorylate the phosphosites on Ste5 in the presence of the kinase Fus3.

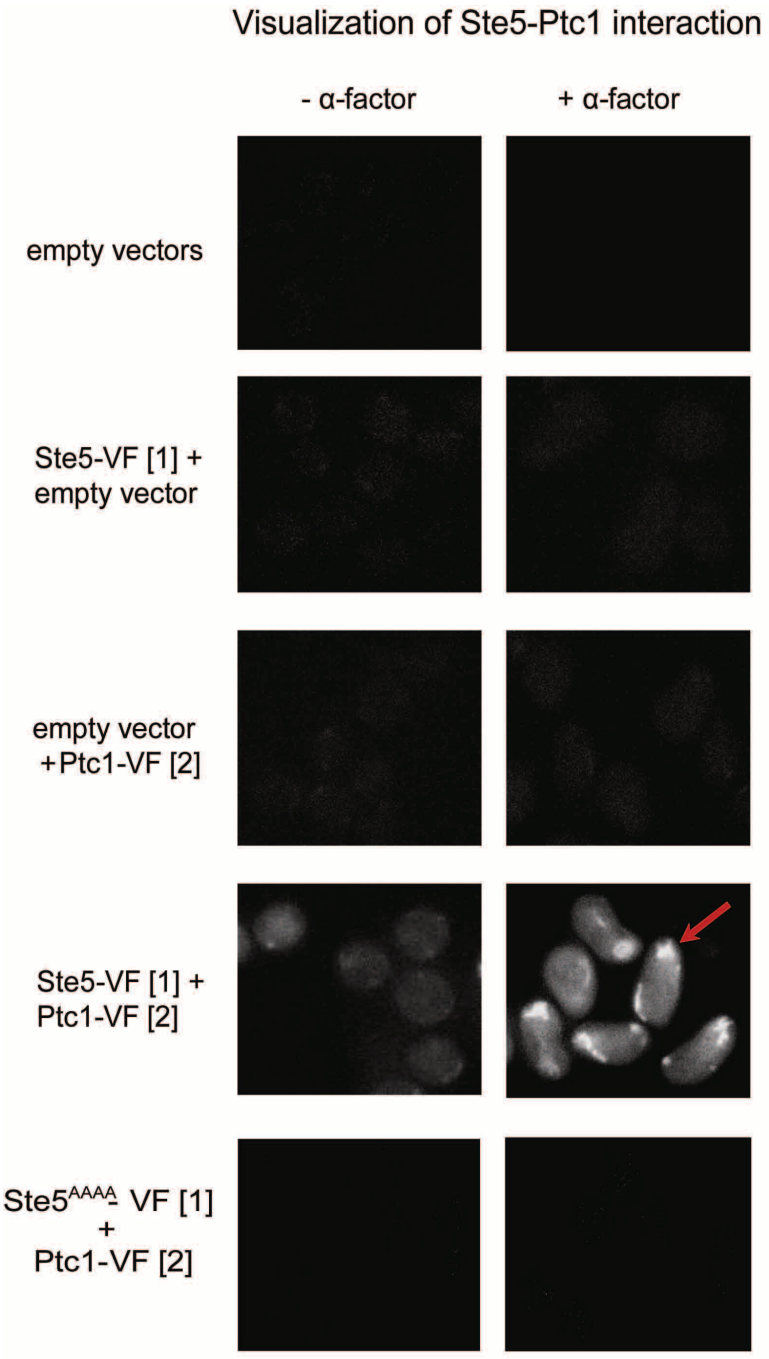

Supplementary Figure 20 Detection of Ste5-Ptc1 interaction using Venus PCA

Detection of the Ste5-Ptc1 interaction and visualization of its cellular location. No detectable signal was observed with the fragments alone. While there is minimal interaction when both proteins fused to fragments are present in the absence of α-factor, significant signal was observed in the presence of α-factor. The signal also localized to the region of polarization (arrow). The lower panel indicates the results with the Ste5 mutant ($Ste5^{AAAA}$; amino acids 277 to 280 mutated to alanine). These results indicate that Ptc1 is recruited to Ste5 at the shmooing region in an α-factor dependent manner.

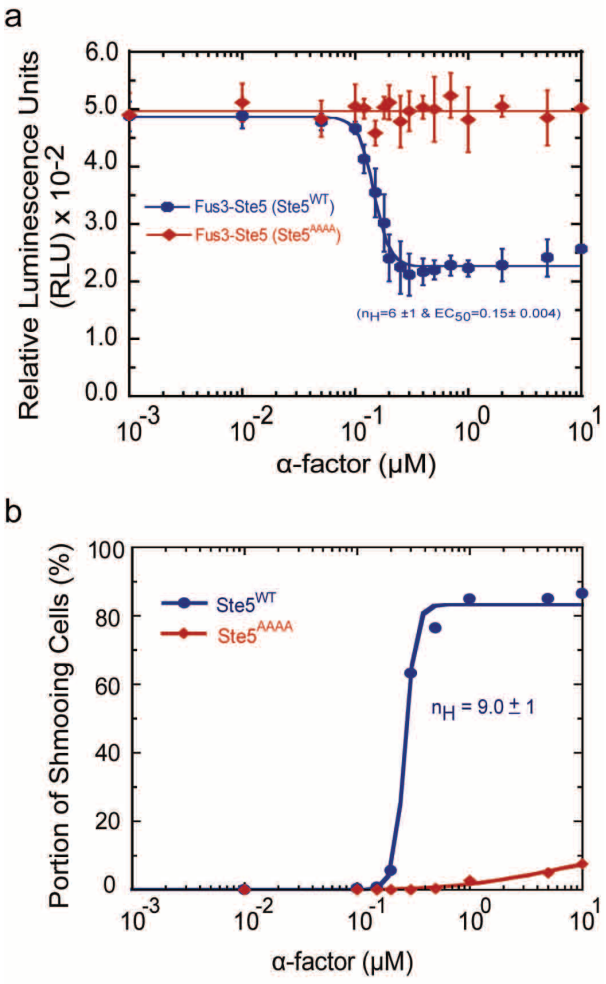

Supplementary Figure 21 The steady-state levels of the Fus3-Ste5 complex and shmooing in *ste5Δ* cells with the Ste5^{AAAA} mutant in comparison to Ste5^{WT}

(a) The Ste5 mutant (Ste5^{AAAA}; amino acids 277 to 280 mutated to alanine) that disrupts the recruitment of Ptc1 to the phosphosites on Ste5 does not interfere with the binding of Fus3 to Ste5, but prevents the Fus3-Ste5 complex from achieving low levels at steady-state.

(b) The fraction of shmooing cells in *wildtype* cells with Ste5^{WT} or with the Ste5 mutant (Ste5^{AAAA}).

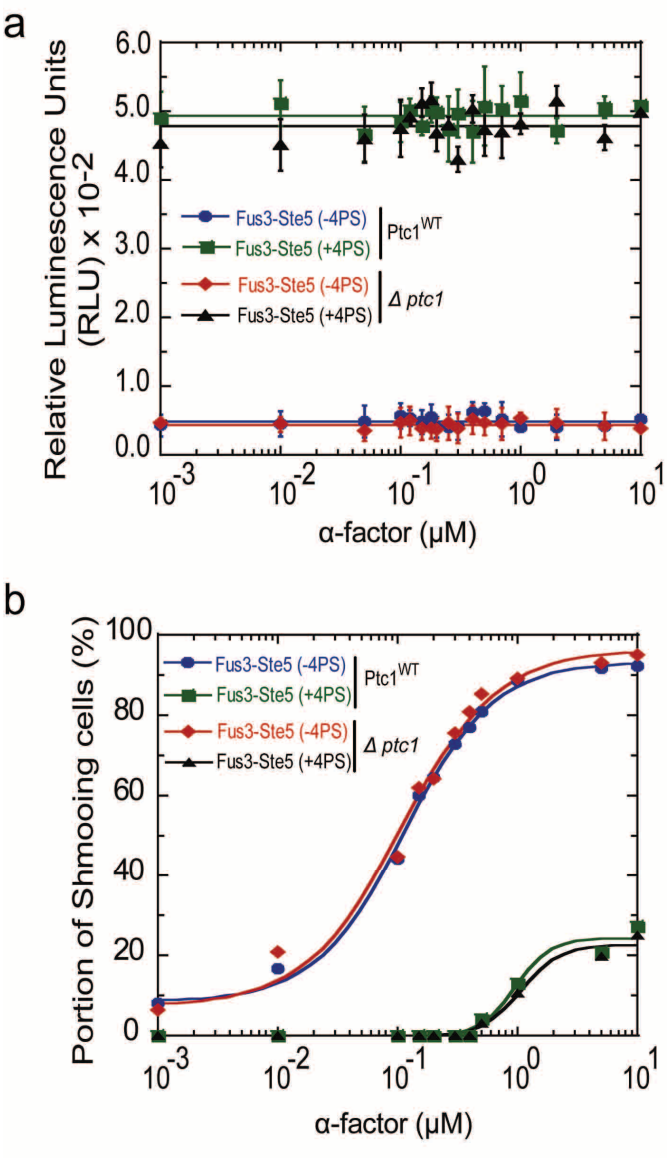

Supplementary Figure 22 The effect of varying the phosphatase Ptc1 on the responses for the phosphosite mutants

(a) and (b) Changes in the steady-state levels of the Fus3-Ste5 complex and shmooing in cells with Ste5 mutants where all phosphorylation sites of Fus3 have been replaced by alanine (-4PS; non-phosphorylatable) or by glutamic acid (+4PS; pseudo-phosphorylated) in the presence ($Ptc1^{WT}$) and absence (*ptc1*Δ) of Ptc1.

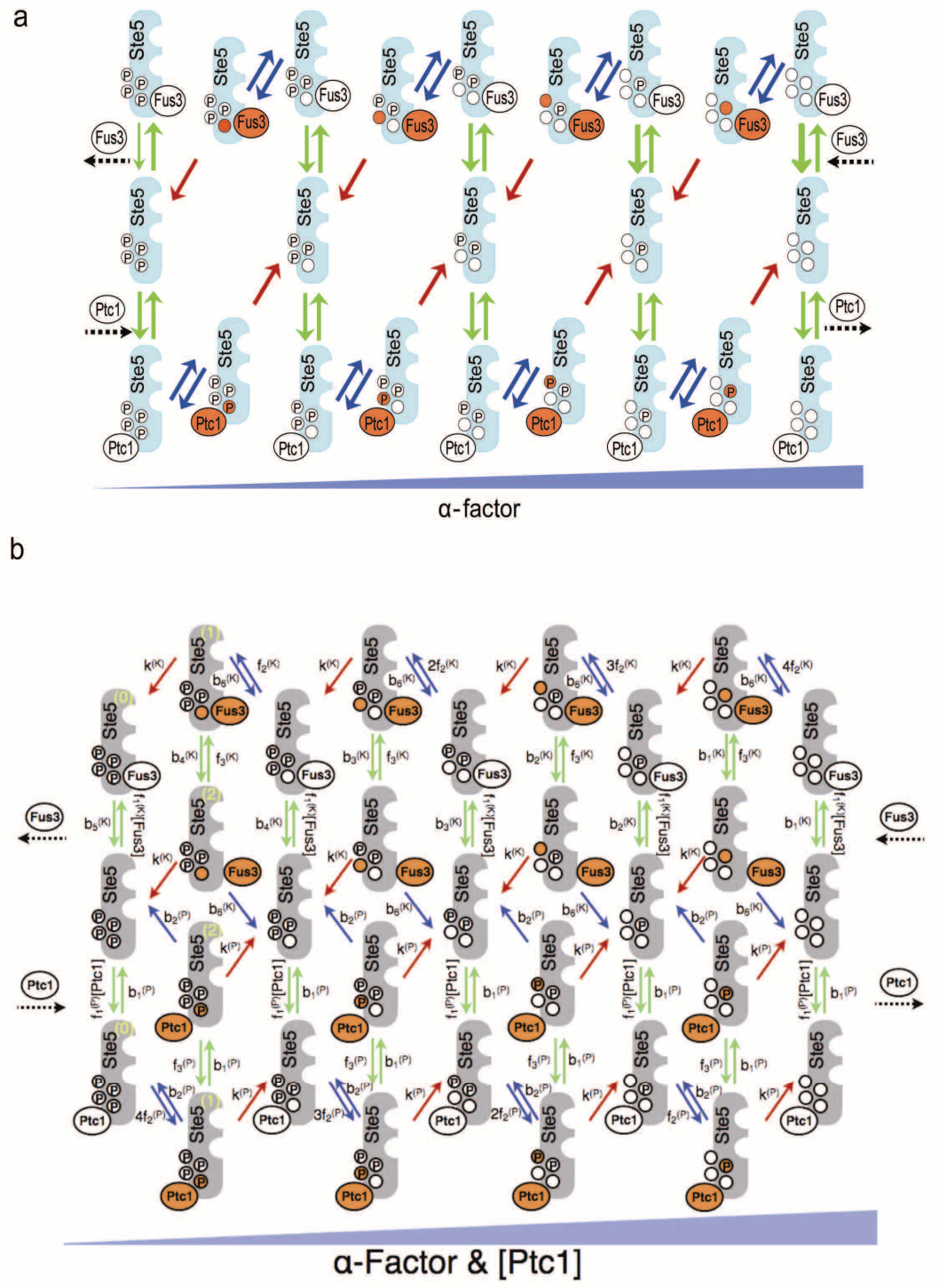

Supplementary Figure 23 Illustration of two versions of the computational model

(a) A model of the switch-like dissociation of the Fus3-Ste5 complex that includes two-stage binding and exhibits zero-order ultrasensitivity. Green arrows; Fus3/Ptc1 binding at their docking site. Blue arrows and white complexes: enzyme–phosphosite binding. Red arrows and orange complexes; catalytic conversion of a phosphosite. Increasing width of green arrows indicate increasing rate of Fus3 dissociation as Ste5 is

less phosphorylated. Data were fit to an equivalent but slightly more complex version of this model as shown in (b).

(b) A general model of Ptc1, Ste5, and Fus3 circuit with two-stage binding that exhibits zero-order ultrasensitivity. We assume that Ste5 has 4 identical phosphosites and that both Fus3 and Ptc1 need to bind Ste5 at a docking site (green arrows) before they can engage in Michaelis-Menton enzymatic reactions with the phosphosites (blue and red arrows). Enzymes interacting with the phosphosites are highlighted in orange. This model is slightly more general than the model presented in (a). Here we assume enzymes can dissociate from the docking motif while bound to the phosphosites. The numbers (0), (1) and (2) specify three types of enzyme-substrate complexes (see Supplementary Information text). All the kinetic rates are given in Supplementary Table 3.

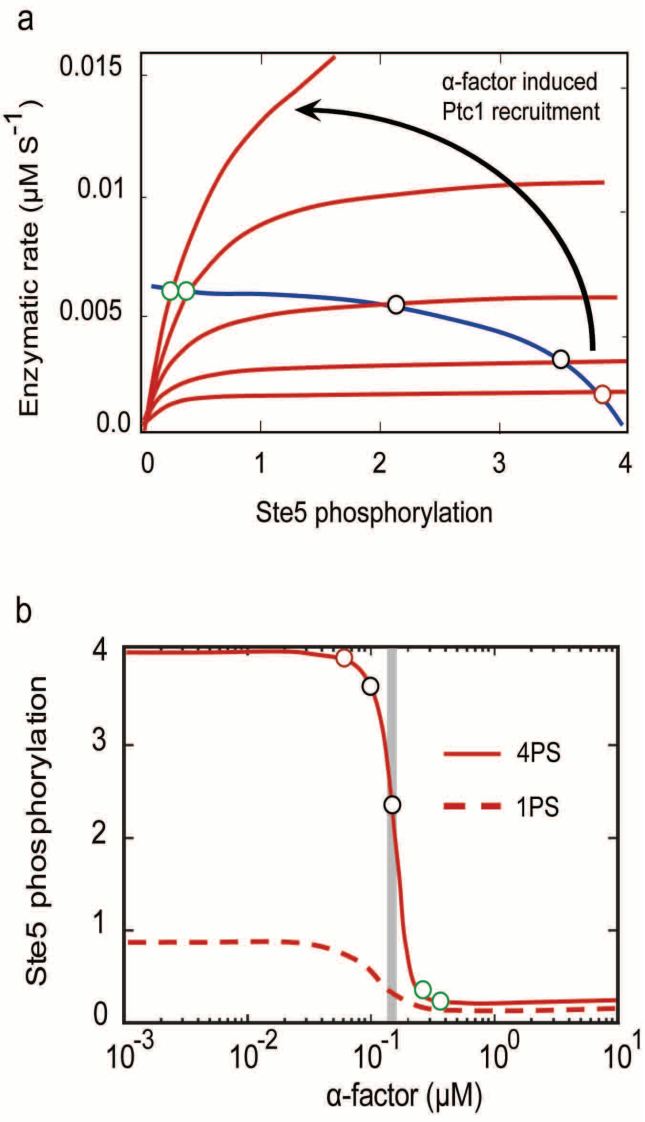

Supplementary Figure 24 Zero-order enzymatic rates explain the switch-like drop in Ste5 phosphorylation level with an increase of local Ptc1 concentration

(a) Predicted enzymatic rates as a function of the average number of phosphorylated phosphosites on Ste5. The activity curve for Fus3 at its endogenous concentration (blue) is shown with 5 activity curves for Ptc1 (red) at increasing concentrations of α-factor (arrow). Points of intersection of the Fus3 and Ptc1 activity curves (open circles) determine the mean steady-state phosphorylation of Ste5, which goes from complete phosphorylation (red) to complete de-phosphorylation (green).

(b) Mean steady-state number of phosphorylated phosphosites on Ste5 (from 3c) *versus* α-factor concentration. We show Ste5 with four (solid line) or one (dashed line) phosphosites. At the threshold concentration of α-factor (grey bar), sufficient Ptc1 is bound to Ste5 to saturate the activity of Fus3 and drive the mean phosphorylation of the phosphosites towards zero (Supplementary Figure 25a). These simulations are done using the model of Supplementary Figure 23b with the fitted parameters.

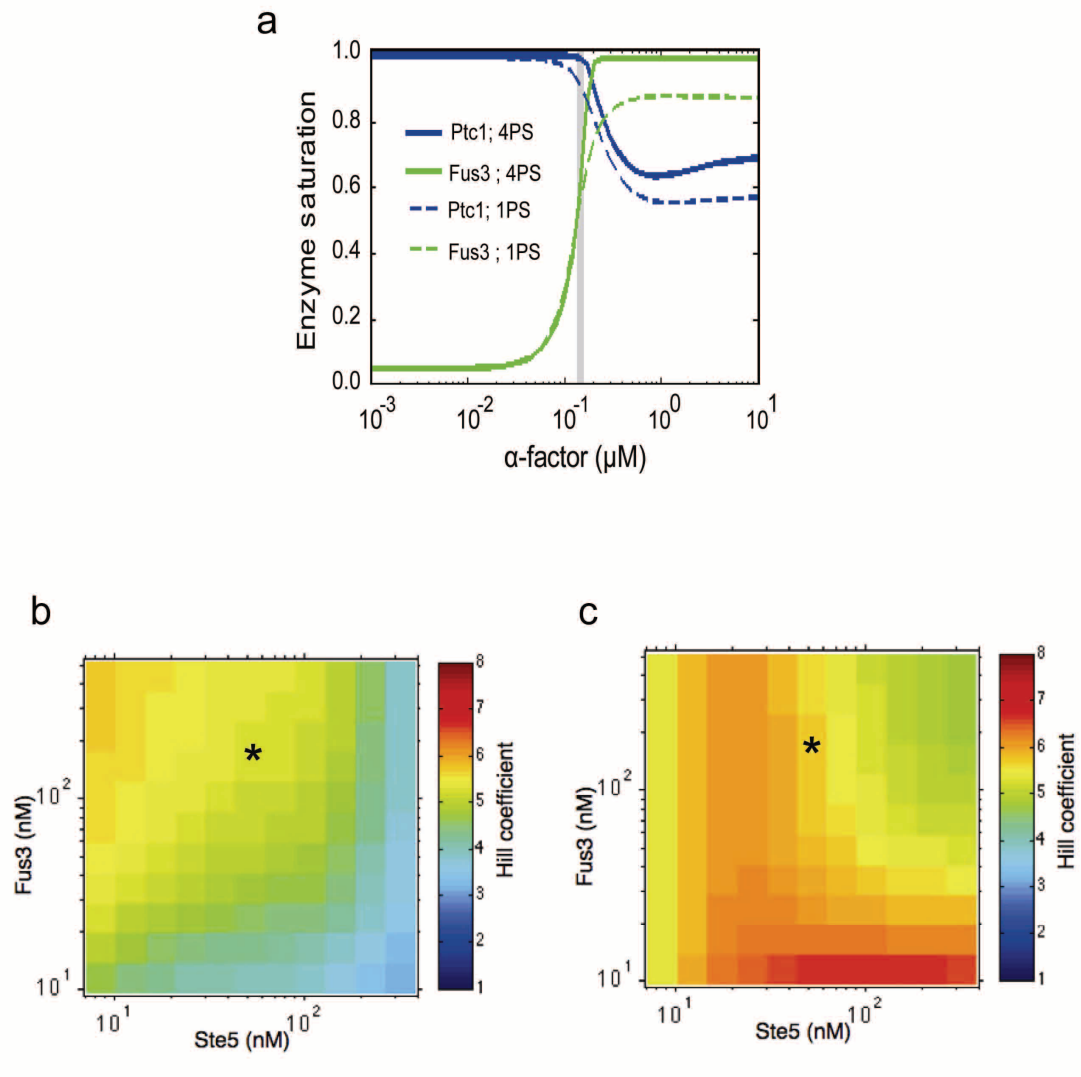

Supplementary Figure 25 Predictions for enzyme saturation, robustness of steric hinderance and zero-order mechanisms.

(a) Enzyme (Fus3 and Ptc1) saturation (the ratio of bound to phosphosites to free enzyme) as a function α-factor concentration for Ste5 with either four phosphosites (4PS; solid lines) or a single site (1PS; dashed lines) predicted using the full model of Supplementary Figure 23b. Grey bar specifies the threshold concentration of α-factor.

(b) and (c) Heat maps of the Hill coefficients obtained for two modifications of the model. Each pixel represents the value of the Hill coefficient determined from a dose response of α-factor at given concentrations of Fus3 and Ste5. (b) A one-stage model based on the model of supplementary Figure 23b with parameters that allow only steric hinderance. (c) A two-stage model based on the model of Supplementary Figure 23b with parameters that allow only zero-order ultrasensitivity.

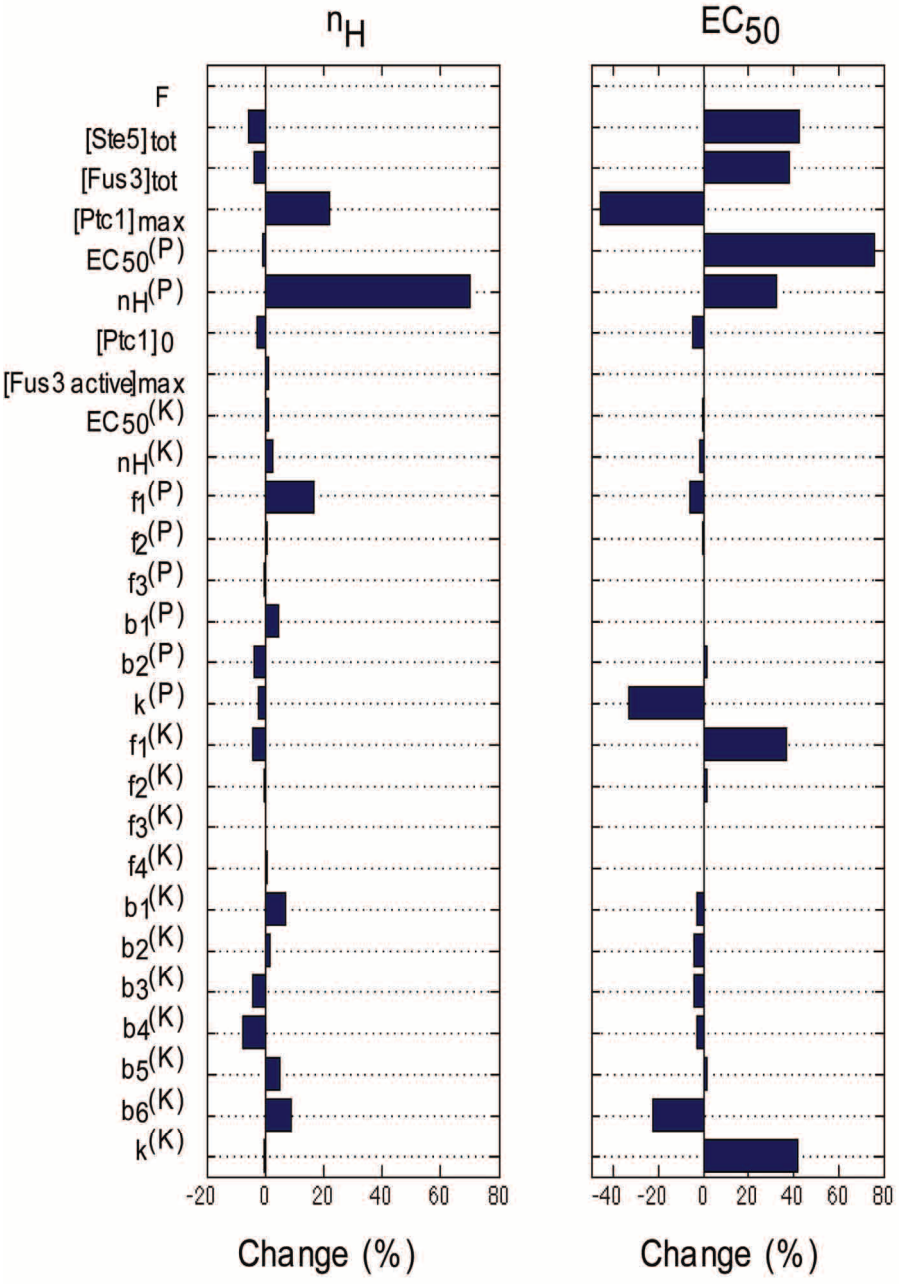

Supplementary Figure 26 Sensitivity analysis of the model

Sensitivity of the n_H and EC_{50} for a switch-like change in phosphorylation of Ste5 to variations in the model parameters. The mean absolute percentage change in the Hill coefficient (n_H) and EC_{50} is shown as each parameter is either multiplied or divided by 2. A negative change denotes a decrease and a positive change an increase in n_H and EC_{50} as the parameter increased.

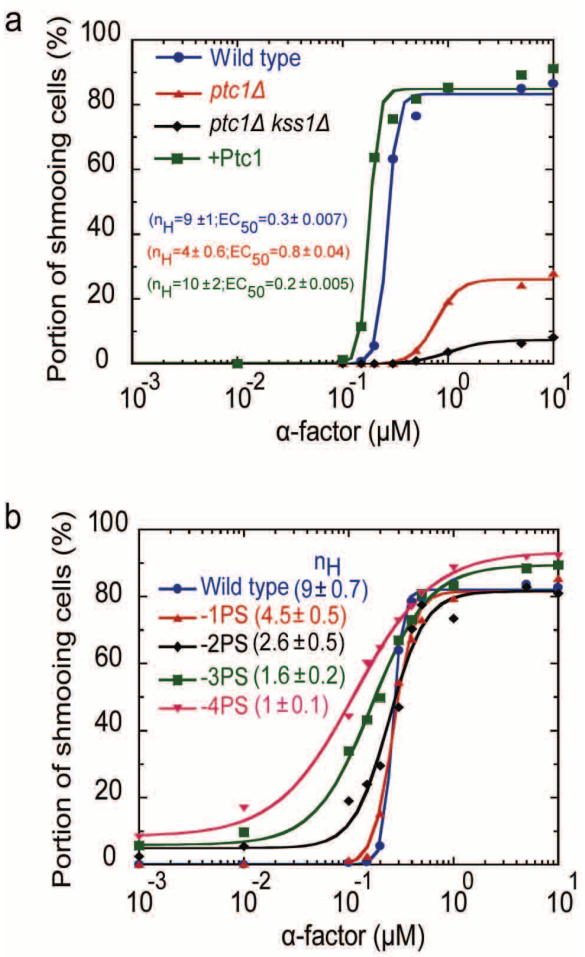

Supplementary Figure 27 Experimental validations of robust zero-order ultrasensitivity model predictions

Changes in the fraction of shmooing cells (a), upon varying the Ptc1 concentration *in-vivo*. We used *wildtype* (WT), Ptc1 knockout (*ptc1Δ*) and a strain over-expressing Ptc1 (+Ptc1). A double deletion of *ptc1Δ kss1Δ* abolished the shmooing observed with *ptc1Δ* alone. Analysis of switching of the shmooing (b) as a function of α-factor using single (-1PS: AbCD), double (-2PS: abCD), triple (-3PS: Abcd) or quadruple (-4PS: abcd) non-phosphorylatable mutants of Ste5. The Hill coefficient, EC_{50} and their errors are calculated from fits of the data to a Hill function (solid lines).

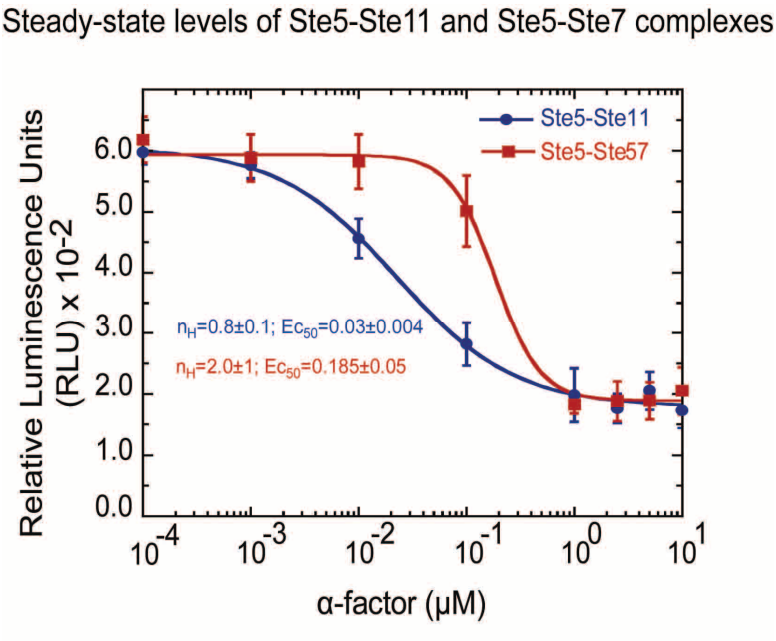

Supplementary Figure 28 Steady-state levels of the Ste5-Ste11 and Ste5-Ste7 complexes

Rluc PCA response curves for the steady state levels of Ste5-Ste11 and Ste5-Ste7 complexes with increasing α-factor concentrations. Data were fit to Hill function (solid lines). Steady-state levels of the Ste5-Ste11 complex change in a graded manner while levels of the Ste5-Ste7 complex change ultrasensitively.

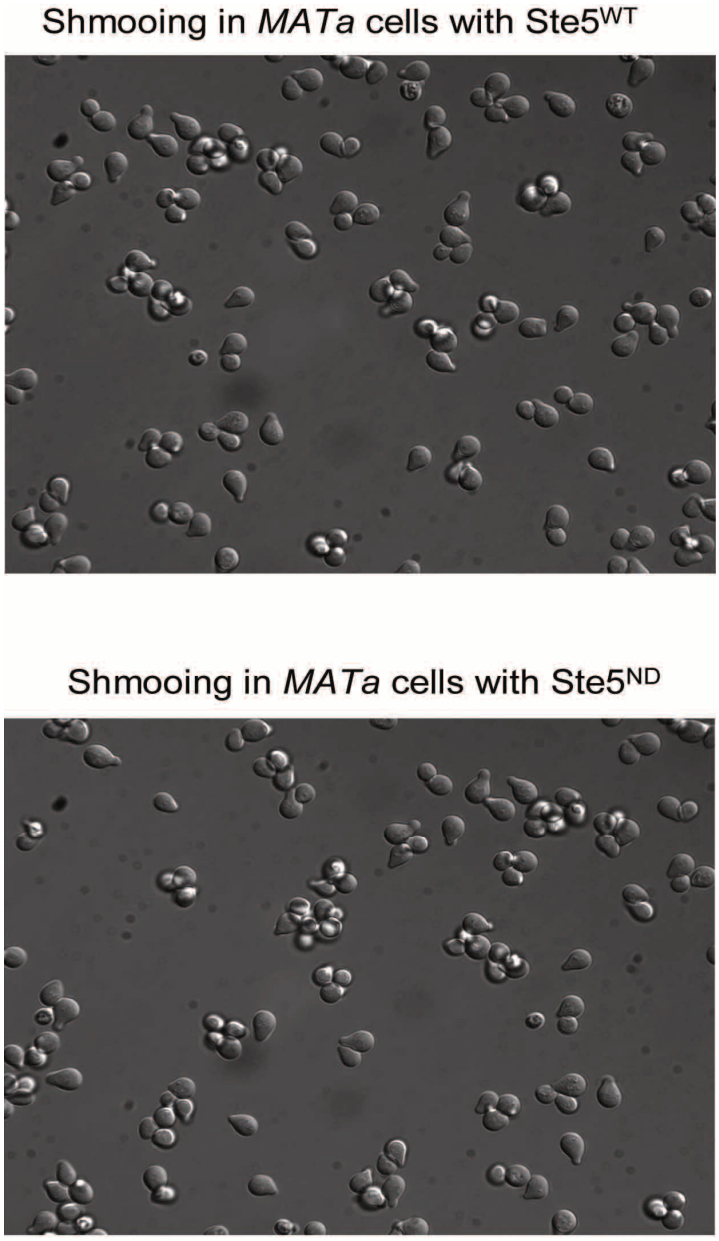

Supplementary Figure 29 Images to show the shmooing types in *Ste5Δ* cells carrying either Ste5^{WT} or Ste5ND. Shmooing phenotype is identical in both Ste5^{WT} and Ste5ND.

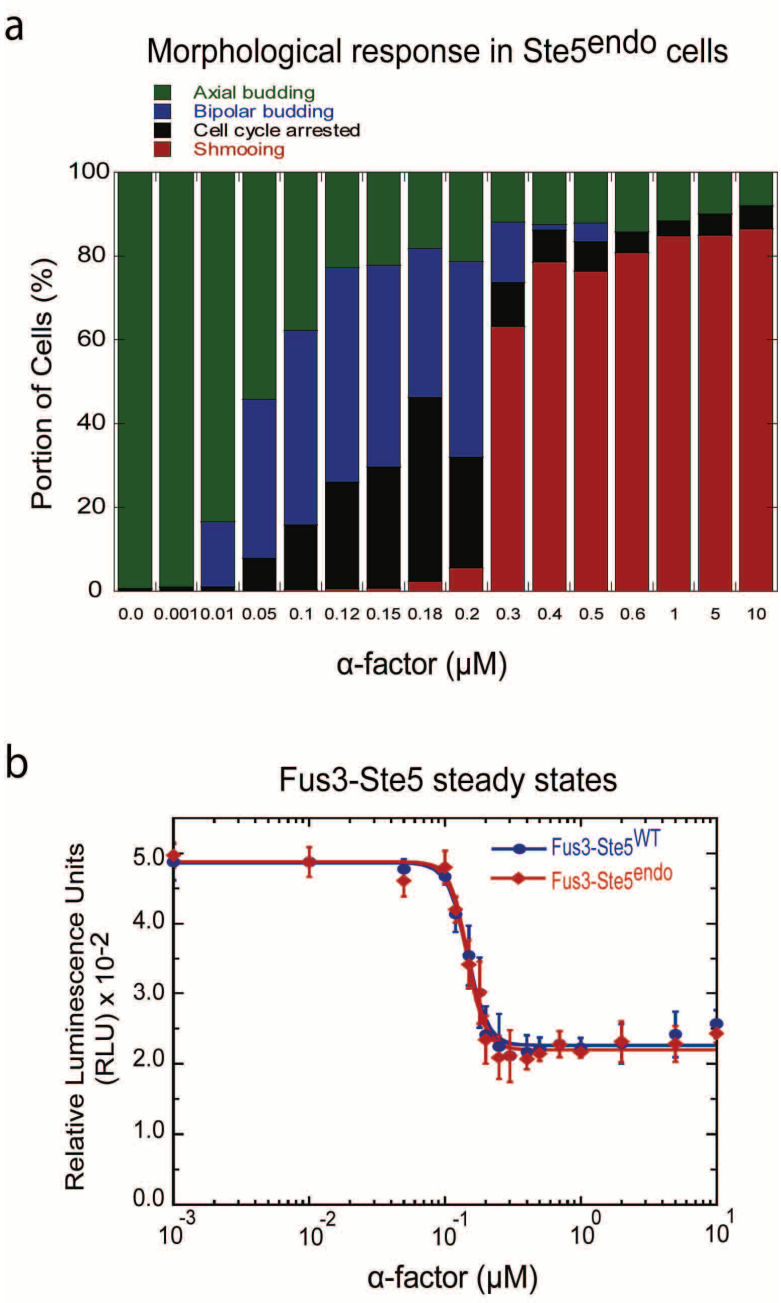

Supplementary Figure 30 Response profiles with endogenously tagged Ste5

(a) Morphological response in cells with endogenously tagged Ste5 (Ste5-Rluc F[2]).

(b) Fus3-Ste5 steady states in cells with endogenously tagged Ste5 (Ste5-Rluc F[2]).

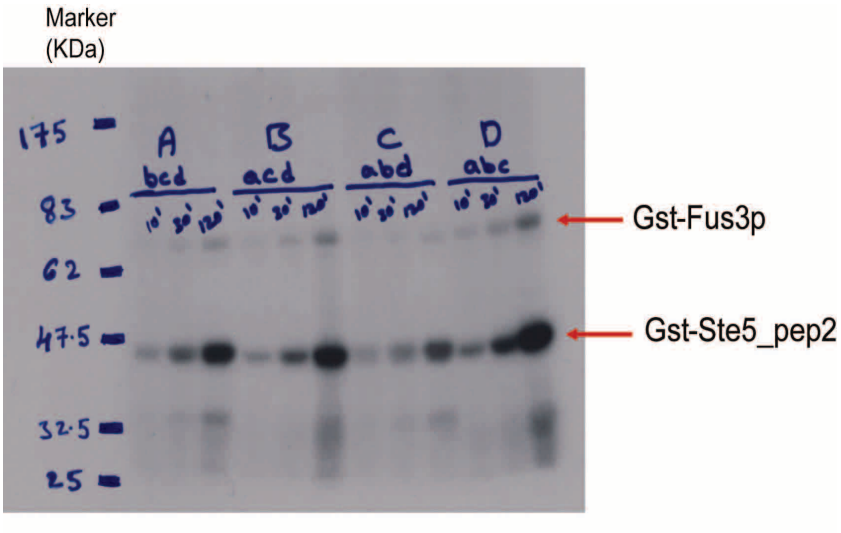

Supplementary Figure 31 Phosphorylations on Gst-Ste5_pep2 phosphosites are distinct from phosphorylation on Gst-Fus3.

Scan of the original in vitro kinase assay blot to show distinction of molecular weights of Gst-Fus3 (~67 KDa) and Gst-Ste5_pep2 (~40 KDa).

Supplementary tables

Supplementary Table 1: List of plasmids used in this study

VF[1]-Venus fragment 1, VF[2]-Venus fragment 2 and VFL-Venus full length

Plasmid	Parent Vector	Promoter	Description
pAG25-RlucF[1]	pAG25		RlucF[1] cassette
pAG32-RlucF[2]	pAG32		RlucF[2] cassette
pMM50	p413	TEF	nNOS-RlucF[1]
pMM51	p415	TEF	aSyn-RlucF[2]
pSH95	pRS316	Ste5 native	$Ste5^{WT}$ (Bhattacharyya et.al., 2006)
pRB200	pRS316	Ste5 native	$Ste5^{ND}$ (Bhattacharyya et.al., 2006)
pRB200-MM300	pRS316	Ste5 native	$Ste5^{ND}$ – RlucF[2]
pSH95-MM100	pRS316	Ste5 native	ABCD ($Ste5^{WT}$ – RlucF[2])
pSH95-MM101	pRS316	Ste5 native	aBCD ($Ste5^{T267V}$ – RlucF[2])
pSH95-MM102	pRS316	Ste5 native	AbCD ($Ste5^{S276A}$ - Rluc[F])
pSH95-MM103	pRS316	Ste5 native	ABcD ($Ste5^{T287V}$ - RlucF[2])
pSH95-MM104	pRS316	Ste5 native	ABCd ($Ste5^{S329A}$ – RlucF[2])
pSH95-MM105	pRS316	Ste5 native	abCD ($Ste5^{T267V,S276A}$ – RlucF[2])
pSH95-MM106	pRS316	Ste5 native	AbcD ($Ste5^{S276A,T287V}$ – RlucF[2])
pSH95-MM107	pRS316	Ste5 native	ABcd ($Ste5^{T287V,S329A}$ – RlucF[2])
pSH95-MM108	pRS316	Ste5 native	aBcD ($Ste5^{T267V,T287V}$ – RlucF[2])
pSH95-MM109	pRS316	Ste5 native	aBCd ($Ste5^{T267V,S329A}$ – RlucF[2])
pSH95-MM110	pRS316	Ste5 native	AbCd ($Ste5^{S276A,S329A}$ – RlucF[2])
pSH95-MM111	pRS316	Ste5 native	Abcd ($Ste5^{S276A,T287V,S329A}$ – RlucF[2])
pSH95-MM112	pRS316	Ste5 native	aBcd ($Ste5^{T267V,T287V,S329A}$ – RlucF[2])
pSH95-MM113	pRS316	Ste5 native	abCd ($Ste5^{T267V,S276A,S329A}$ – RlucF[2])
pSH95-MM114	pRS316	Ste5 native	abcD ($Ste5^{T267V,S276A,T287V}$ – RlucF[2])
pSH95-MM115	pRS316	Ste5 native	abcd ($Ste5^{T267V,S276A,T287V,S329A}$ – RlucF[2])
pSH95-MM116	pRS316	Ste5 native	Ebcd ($Ste5^{T267E,S276A,T287V,S329A}$ – RlucF[2])
pSH95-MM117	pRS316	Ste5 native	aFcd ($Ste5^{T267V,S276E,T287V,S329A}$ – RlucF[2])
pSH95-MM118	pRS316	Ste5 native	abGd ($Ste5^{T267V,S276A,T287E,S329A}$ – RlucF[2])
pSH95-MM119	pRS316	Ste5 native	abcH ($Ste5^{T267V,S276A,T287V,S329E}$ – RlucF[2])
pSH95-MM120	pRS316	Ste5 native	EFcd ($Ste5^{T267E,S276E,T287V,S329A}$ – RlucF[2])
pSH95-MM121	pRS316	Ste5 native	EbGd ($Ste5^{T267E,S276A,T287E,S329A}$ – RlucF[2])
pSH95-MM122	pRS316	Ste5 native	EbcH ($Ste5^{T267E,S276A,T287V,S329H}$ – RlucF[2])
pSH95-MM123	pRS316	Ste5 native	aFGd ($Ste5^{T267V,S276E,T287E,S329A}$ – RlucF[2])
pSH95-MM124	pRS316	Ste5 native	aFcH ($Ste5^{T267V,S276E,T287V,S329H}$– RlucF[2])
pSH95-MM125	pRS316	Ste5 native	abGH ($Ste5^{T267V,S276A,T287E,S329E}$ – RlucF[2])

Plasmid	Parent Vector	Promoter	Description
pSH95-MM126	pRS316	Ste5 native	EFGd (Ste5^{T267E,S276E,T287E,S329A} – RlucF[2])
pSH95-MM127	pRS316	Ste5 native	EbGH (Ste5^{T267E,S276A,T287E,S329E} – RlucF[2])
pSH95-MM128	pRS316	Ste5 native	aFGH (Ste5^{T267V,S276E,T287E,S329E} – RlucF[2])
pSH95-MM129	pRS316	Ste5 native	EFcH (Ste5^{T267E,S276E,T287V,S329E} – RlucF[2])
pSH95-MM130	pRS316	Ste5 native	EFGH (Ste5^{T267E,S276E,T287E,S329E} – RlucF[2])
pSH95-MM131	pRS316	Ste5 native	EBCD (Ste5^{T267E,S276,T287,S329} – RlucF[2])
pSH95-MM132	pRS316	Ste5 native	AFCD (Ste5^{T267,S276E,T287,S329} – RlucF[2])
pSH95-MM133	pRS316	Ste5 native	ABGD (Ste5^{T267,S276,T287E,S329} – RlucF[2])
pSH95-MM134	pRS316	Ste5 native	ABCH (Ste5^{T267,S276,T287,S329E} – RlucF[2])
pSH95-MM135	pRS316	Ste5 native	Ste5^{*AAAA} (Ste5^{P277A,L278A,L279A,P280A})
pSH95-MM136	pRS316	Ste5 native	ABCD (Ste5^{WT} – VFL)
pSH95-MM137	pRS316	Ste5 native	aBCD (Ste5^{T267V} – VFL)
pSH95-MM138	pRS316	Ste5 native	AbCD (Ste5^{S276A} - VFL)
pSH95-MM139	pRS316	Ste5 native	ABcD (Ste5^{T287V} - VFL)
pSH95-MM140	pRS316	Ste5 native	ABCd (Ste5^{S329A} – VFL)
pSH95-MM141	pRS316	Ste5 native	abCD (Ste5^{T267V,S276A} – VFL)
pSH95-MM142	pRS316	Ste5 native	ABcd (Ste5^{T287V,S329A} – VFL)
pSH95-MM143	pRS316	Ste5 native	Abcd (Ste5^{S276A,T287V,S329A} – VFL)
pSH95-MM144	pRS316	Ste5 native	abcD (Ste5^{T267V,S276A,T287V} – VFL)
pSH95-MM145	pRS316	Ste5 native	abcd (Ste5^{T267V,S276A,T287V,S329A} – VFL)
pRB200-MM146	pRS316	Ste5 native	Ste5ND – VFL
pMM60	p415	ADH	Ptc1
pMM61	p413	ADH	Ste5-L-VF [1]
pMM62	p413	ADH	Ste5*(Ste5^{P277A,L278A,L279A,P280A})-L-VF [1]
pMM63	p415	ADH	Ptc1-L-VF [2]
pMM200	pGEX-5X-3		GST-Fus3
pMM210	pGEX-5X-3		GST-Ste5_pep2 $^{(214-334)}$ (ABCD-WT)
pMM211	pGEX-5X-3		GST-Ste5_pep2 $^{(214-334)}$ (Abcd)
pMM212	pGEX-5X-3		GST-Ste5_pep2 $^{(214-334)}$ (aBcd)
pMM213	pGEX-5X-3		GST-Ste5_pep2 $^{(214-334)}$ (abCd)
pMM214	pGEX-5X-3		GST-Ste5_pep2 $^{(214-334)}$ (abcD)
pMM215	pGEX-5X-3		GST-Ste5_pep2 $^{(214-334)}$ (abcd)
pMM216	pMAL-c2x		MBP-Ptc1
pMM217	pMAL-c2x		MBP-Fus3
pMM250	pRS316	Ste5 native	Ste5^{AAAA} (Ste5^{P277A,L278A,L279A,P280A}) - RlucF[2]

Supplementary Table 2: List of yeast strains used in this study

Strain	Description
BY4741	*MATa his3Δ leu2Δ met15Δ ura3Δ*
MM001	BY4741 *FUS3* - L- RlucF[1]
MM002	BY4741 *FUS3*-L-RlucF[1] *STE5*-L-RlucF[2]
MM003	BY4741 *ste5Δ FUS3* - L- RlucF[1]
MM004	BY4741 *ptc1Δ FUS3* - L- RlucF[1]
MM005	BY4741 *ptc1Δ FUS3* - L- RlucF[1] *STE5*-L-RlucF[2]
MM006	BY4741 *FUS3(K42R)*-L-RlucF[1] *STE5*-L-RlucF[2]
MM007	BY4741 *STE5*-L-RlucF[1] *PTC1*-L-RlucF[2]
MM008	BY4741 *STE5*-L-RlucF[1] *STE11*-L-RlucF[2]
MM007	BY4741 *STE5*-L-RlucF[1] *STE7*-L-RlucF[2]
MM010	BY4741 *ste5Δ ptc1Δ FUS3* - L- RlucF[1]
BY4741 *fus3Δ*	
BY4741 *kss1Δ*	
BY4741 *hog1Δ*	
BY4741 *ptc1Δ*	
BY4741 *ptc1Δ kss1Δ*	
BY4741 *ppz1Δ*	
BY4741 *ppz2Δ*	
BY4741 *sal6Δ*	
BY4741 *pph21Δ*	
BY4741 *pph22Δ*	
BY4741 *ppg1Δ*	
BY4741 *cna1Δ*	
BY4741 *cna2Δ*	
BY4741 *ppt1Δ*	
BY4741 *ptc3Δ*	
BY4741 *ptc4Δ*	
BY4741 *ptc6Δ*	
BY4741 *ptc5Δ*	
BY4741 *ptp1Δ*	
BY4741 *ptp3Δ*	
BY4741 *mih1Δ*	
BY4741 *ltp1Δ*	
BY4741 *pps1Δ*	
BY4741 *tep1Δ*	
BY4741 *sdp1Δ*	
BY4741 *ymr1Δ*	
BY4741 *msg5Δ*	
BY4741 *ptp2Δ*	
BY4741 *pph3Δ*	
BY4741 *ptc2Δ*	

Supplementary Table 3: List of all parameters used in the model

Parameter	Value	Error (%)
F	0.2	not fitted
$[Ste5]_{tot}$	52(nM)	not fitted
$[Fus3]_{tot}$	197(nM)	not fitted
$[Ptc1]_{max}$	39(nM)	33
$EC_{50}^{(P)}$	240(nM)	17
$n_H^{(P)}$	2.3	18
$[Ptc1]_0$	1.2(nM)	25
$[Fus3_{active}]_{max}$	5.8(nM)	21
$EC_{50}^{(K)}$	1680(nM)	26
$n_H^{(K)}$	1.3	23
$f_1^{(P)}$	186000 $nM^{-1}s^{-1}$	35
$f_2^{(P)}$	327 s^{-1}	34
$f_3^{(P)}$	0.3 s^{-1}	31
$b_1^{(P)}$	22 s^{-1}	18
$b_2^{(P)}$	0.12 s^{-1}	35
$k^{(P)}$	0.5 s^{-1}	30
$f_1^{(K)}$	12000 $nM^{-1}s^{-1}$	24
$f_2^{(K)}$	850 s^{-1}	35
$f_3^{(K)}$	0.1 s^{-1}	31
$f_4^{(K)}$	109000 $nM^{-1}s^{-1}$	28
$b_1^{(K)}$	99 s^{-1}	25
$b_2^{(K)}$	42 s^{-1}	25
$b_3^{(K)}$	21 s^{-1}	25
$b_4^{(K)}$	13 s^{-1}	25
$b_5^{(K)}$	10 s^{-1}	25
$b_6^{(K)}$	24 s^{-1}	28
$k^{(K)}$	1.13 s^{-1}	28

Except for the first three parameters, all others were obtained by fitting the model predictions to the experimental data using a Markov chain Monte Carlo method. The best-fit parameters were found through extensive fitting of the data by a combination of trial-and-error and Monte Carlo methods. The errors shown as the standard deviation as a percentage of the mean represent the standard deviation of the parameters over a Monte Carlo run, where the parameters were restricted to vary only within a factor of 2 from their best-fit values.

Supplementary references

31 Tarassov, K. *et al.* An in Vivo Map of the Yeast Protein Interactome. *Science* (2008).

32 Harris, B. Z., Hillier, B. J. & Lim, W. A. Energetic determinants of internal motif recognition by PDZ domains. *Biochemistry* **40**, 5921-5930 (2001).

33 Ghaemmaghami, S. *et al.* Global analysis of protein expression in yeast. *Nature* **425**, 737-741 (2003).

34 Sheff, M. A. & Thorn, K. S. Optimized cassettes for fluorescent protein tagging in Saccharomyces cerevisiae. *Yeast* **21**, 661-670 (2004).

35 Andersson, J. *et al.* Differential input by Ste5 scaffold and Msg5 phosphatase route a MAPK cascade to multiple outcomes. *Embo J* **23**, 2564-2576 (2004).

36 Remenyi, A., Good, M. C., Bhattacharyya, R. P. & Lim, W. A. The role of docking interactions in mediating signaling input, output, and discrimination in the yeast MAPK network. *Mol Cell* **20**, 951-962 (2005).

37 Salazar, C. & Hofer, T. Kinetic models of phosphorylation cycles: a systematic approach using the rapid-equilibrium approximation for protein-protein interactions. *Biosystems* **83**, 195-206 (2006).

38 Gunawardena, J. Multisite protein phosphorylation makes a good threshold but can be a poor switch. *Proc Natl Acad Sci U S A* **102**, 14617-14622 (2005).

39 Markevich, N. I., Hoek, J. B. & Kholodenko, B. N. Signaling switches and bistability arising from multisite phosphorylation in protein kinase cascades. *J Cell Biol* **164**, 353-359 (2004).

40 Maeder, C. I. *et al.* Spatial regulation of Fus3 MAP kinase activity through a reaction-diffusion mechanism in yeast pheromone signalling. *Nat Cell Biol* **9**, 1319-1326 (2007).

41 Shahrezaei, V., Ollivier, J. F. & Swain, P. S. Colored extrinsic fluctuations and stochastic gene expression. *Mol Syst Biol* **4**, 196 (2008).

42 Feinerman, O. *et al.* Variability and robustness in T cell activation from regulated heterogeneity in protein levels. *Science* **321**, 1081-1084 (2008).